AD-A192 330 AN ANALYSIS OF HORIZONTAL TEMPERATURE GRADIENTS AND HEAT CONTENT IN THE M..(U) NAVAL POSTGRADUATE SCHOOL MONTEREY CA J J MURRAY DEC 87 1/1

UNCLASSIFIED F/G 8/3 NL

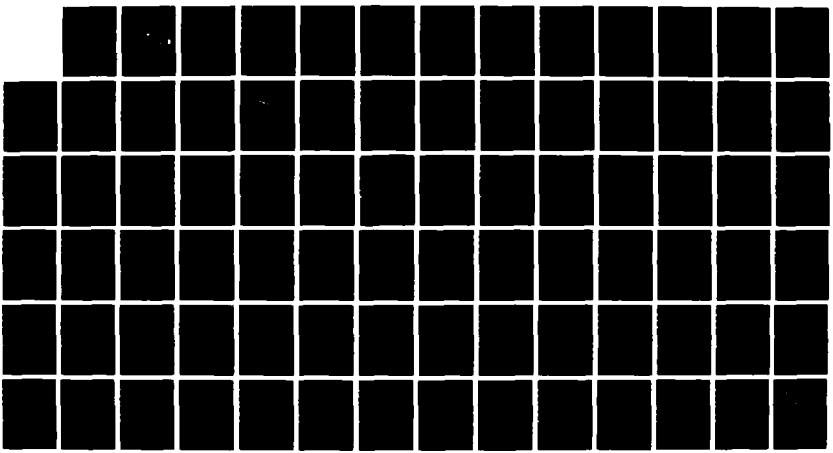

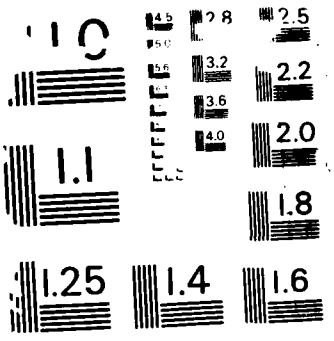

RESOLUTION TEST CHART
NATIONAL BUREAU OF STANDARDS-1963

NAVAL POSTGRADUATE SCHOOL
Monterey, California

THESIS

AN ANALYSIS OF HORIZONTAL TEMPERATURE GRADIENTS AND HEAT CONTENT IN THE MIXED LAYER AND OF THE SURFACE FORCING DURING PATCHEX

by

John J. Murray

December 1987

Thesis Advisor Timothy P. Stanton

 A192330

REPORT DOCUMENTATION PAGE

1a. REPORT SECURITY CLASSIFICATION UNCLASSIFIED	1b RESTRICTIVE MARKINGS NONE
2a. SECURITY CLASSIFICATION AUTHORITY N/A	3 DISTRIBUTION / AVAILABILITY OF REPORT Approved for public release; distribution is unlimited.
2b. DECLASSIFICATION / DOWNGRADING SCHEDULE	
4. PERFORMING ORGANIZATION REPORT NUMBER(S)	5. MONITORING ORGANIZATION REPORT NUMBER(S)
6a NAME OF PERFORMING ORGANIZATION Naval Postgraduate School 6b OFFICE SYMBOL (*If applicable*) Code 68	7a. NAME OF MONITORING ORGANIZATION Naval Postgraduate School
6c. ADDRESS (*City, State, and ZIP Code*) Monterey, CA 93943-5000	7b. ADDRESS (*City, State, and ZIP Code*) Monterey, CA 93943-5000
8a. NAME OF FUNDING / SPONSORING ORGANIZATION 8b. OFFICE SYMBOL (*If applicable*)	9. PROCUREMENT INSTRUMENT IDENTIFICATION NUMBER
8c. ADDRESS (*City, State, and ZIP Code*)	10. SOURCE OF FUNDING NUMBERS PROGRAM ELEMENT NO. / PROJECT NO. / TASK NO / WORK UNIT ACCESSION NO.

11. TITLE (*Include Security Classification*)
AN ANALYSIS OF HORIZONTAL TEMPERATURE GRADIENTS AND HEAT CONTENT IN THE MIXED LAYER AND OF THE SURFACE FORCING DURING PATCHEX (UNCLASSIFIED)

12. PERSONAL AUTHOR(S)
Murray, John J.

13a. TYPE OF REPORT	13b. TIME COVERED	14. DATE OF REPORT (*Year, Month, Day*)	15. PAGE COUNT
Master's Thesis	FROM _____ TO _____	1987 December	81

16. SUPPLEMENTARY NOTATION

17. COSATI CODES			18. SUBJECT TERMS (*Continue on reverse if necessary and identify by block number*)
FIELD	GROUP	SUB-GROUP	PATCHEX, surface forcing, mixed layer heat content horizontal temperature gradient, Thesis

19. ABSTRACT (*Continue on reverse if necessary and identify by block number*)

This study is an analysis of high resolution measurements taken during the PATCHEX experiment. PATCHEX was designed to study shear related mixing in the upper thermocline. As a participant in the study, the R/V POINT SUR's contribution was to survey an 8 kilometer square area centered on the R/P FLIP which was moored at 34°N127 °W. The survey which was conducted from 4-16 November 1986, gathered high resolution CTD, microconductivity and current velocity data to allow a detailed analysis of the small scale dynamics and thermohaline structure of the site. This thesis examined a subset of the R/V POINT SUR measurements to describe the vertical and horizontal thermohaline structure, surface fluxes and heat content of the upper 120 meters at the PATCHEX site.

20. DISTRIBUTION / AVAILABILITY OF ABSTRACT	21. ABSTRACT SECURITY CLASSIFICATION
☒ UNCLASSIFIED/UNLIMITED ☐ SAME AS RPT ☐ DTIC USERS	UNCLASSIFIED
22a NAME OF RESPONSIBLE INDIVIDUAL Timothy P. Stanton	22b TELEPHONE (*Include Area Code*) (408) 646-3144 22c OFFICE SYMBOL Code 68St

DD FORM 1473, 84 MAR 83 APR edition may be used until exhausted
All other editions are obsolete

SECURITY CLASSIFICATION OF THIS PAGE

* U.S. Government Printing Office: 1986—606-24.

A two-layer mixed layer system existed during the first half of the study period due to the effects of precipitation, a 0.1 N/m^2 mean wind stress and strong diurnal heating. A 0.04 to 0.06 ppt salt deficit and 0.25°K temperature excess were measured in the surface layer which ranged from 10 to 35 meters depth. The depth of the seasonal mixed layer varied between 42 and 62 meters in response to the internal wave field in the upper thermocline.

Significantly different horizontal gradients were analyzed in the time series of temperature and salinity at 10 meters and 40 meters. This motivated an attempt to map those gradients on to a uniform grid by objective analysis. The horizontal gradients at 10 meterr were determined to decrease most rapidly toward the southeast corner of the survey area. Weaker gradients at 40 meters increased nominally from west to east This further illustrated the decoupling of the upper and lower layers from 6-12 October.

Convective mixing from a 100 W/m^2 mean daily maximum latent heat loss combined with a 75 percent insolation reduction erased the surface layer on 8 and 9 October and continued cooling the entire layer. A net surface heat loss of 35 ± 5 MJ/m^2 (0.7 ± 0.1 MJ/m^2 through the surface) balanced a 0.6 to 0.8 MJ/m^2 overall mixed layer heat loss. This confirmed that the surface flux was the dominant heat transfer mechanism from 8-12 October.

Approved for public release; distribution is unlimited.

An Analysis of Horizontal Temperature Gradients and Heat Content
in the Mixed Layer and of the Surface Forcing During PATCHEX

by

John J. Murray
Lieutenant, United States Navy
B.S., Florida Institute of Technology, 1979

Submitted in partial fulfillment of the
requirements for the degree of

MASTER OF SCIENCE IN METEOROLOGY AND OCEANOGRAPHY

from the

NAVAL POSTGRADUATE SCHOOL
December 1987

Author: John J. Murray
John J. Murray

Approved by: T. P. Stanton
Timothy P. Stanton, Thesis Advisor

Edward B. Thornton
Edward B. Thornton, Second Reader

Curtis A. Collins
Curtis A. Collins, Chairman,
Department of Oceanography

G. E. Schacher
Gordon E. Schacher,
Dean of Science and Engineering

ABSTRACT

This study is an analysis of high resolution measurements taken during the PATCHEX experiment. PATCHEX was designed to study shear related mixing in the upper thermocline. As a participant in the study, the R/V POINT SUR's contribution was to survey an 8 kilometer square area centered on the R/P FLIP which was moored at 34°N127 °W. The survey which was conducted from 4-16 November 1986, gathered high resolution CTD, microconductivity and current velocity data to allow a detailed analysis of the small scale dynamics and thermohaline structure of the site. This thesis examined a subset of the R/V POINT SUR measurements to describe the vertical and horizontal thermohaline structure, surface fluxes and heat content of the upper 120 meters at the PATCHEX site.

A two-layer mixed layer system existed during the first half of the study period due to the effects of precipitation, a 0.1 N/m^2 mean wind stress and strong diurnal heating. A 0.04 to 0.06 ppt salt deficit and 0.25°K temperature excess were measured in the surface layer which ranged from 10 to 35 meters depth. The depth of the seasonal mixed layer varied between 42 and 62 meters in response to the internal wave field in the upper thermocline.

Significantly different horizontal gradients were analyzed in the time series of temperature and salinity at 10 meters and 40 meters. This motivated an attempt to map those gradients on to a uniform grid by objective analysis. The horizontal gradients at 10 meters were determined to decrease most rapidly toward the southeast corner of the survey area. Weaker gradients at 40 meters increased nominally from west to east This further illustrated the decoupling of the upper and lower layers from 6-12 October.

Convective mixing from a 100 W/m^2 mean daily maximum latent heat loss combined with a 75 percent insolation reduction erased the surface layer on 8 and 9 October and continued cooling the entire layer. A net surface heat loss of 35 ± 5 MJ/m^2 (0.7 ± 0.1 MJ/m^3 through the surface) balanced a 0.6 to 0.8 MJ/m^3 overall mixed layer heat loss. This confirmed that the surface flux was the dominant heat transfer mechanism from 8-12 October.

TABLE OF CONTENTS

LIST OF TABLES

LIST OF FIGURES

I. INTRODUCTION

The ocean distributes its heat, salt and momentum through various dynamic and thermodynamic processes. These processes range over scales of seven or more orders of magnitude from basin wide, geostrophic circulations to centimeter or millimeter scales where mechanical energy is viscously dissipated. Studies such as Garrett and Munk (1979) have developed and refined models to investigate the spectral universality of an internal wave base state in the open ocean. Because of the ubiquitous nature of internal waves, their viscous dissipation is believed to play a key role in maintaining the fluxes of heat, salt and momentum in the ocean. Gregg (1984) observed patchy, intermittent mixing events within the well stratified region of the upper thermocline. These events persisted for at least 3 hours at the same depth as a near-inertial internal wave packet. He noted that the average value of ε, the dissipation rate, is relatively low in the upper thermocline and suggested that sustained shear events associated with long period internal waves might provide the most significant source of mechanical mixing energy in that region. Near-inertial internal waves, which are intimately tied to meteorological forcing, would thus play an important role in the production of significant mixing in the upper thermocline.

PATCHEX employed four ships to study turbulent mixing patches associated with significant shear events in the upper thermocline and to relate observations of those patches to the internal wave field. The goals of the experiment as elucidated by Gregg et al (1984) were:

- to describe the nature and spatial distribution of the observed density and velocity fields;
- to discern the spectral nature of the internal wave field in both the frequency and wavenumber domains;
- to observe and quantify the transfer of kinetic energy through the relevant scales and attempt to quantify related changes in potential energy;
- to examine the variability of high wavenumber shear associated with major mixing patches; and
- to refine theories governing the generation and evolution of mixing patches, i.e. to relate average mixing rates to sustained shear events within the highly stratified upper thermocline.

Acknowledging the difficulty in separating the contributions of shear and diffusion from turbulent mixing, the principal investigators decided to examine a horizontally homogeneous site with a simple salinity structure, free from the effects of double diffusion or salt fingering. The limited range of the San Diego based research platform, FLIP, a primary participant and a towed vessel, was also a major concern. FLIP's range limitations clearly created the possiblity of significant diffusive complications associated with mesoscale features near the California Current. A location at a latitude much higher than San Diego was eliminated since the thermocline would be deeper and less accessible as one moved northward. After studying satellite imagery and a review of the ODEX and CALCOFI hydrographic surveys indicated that there were no logistically feasible sites with significantly less horizontal structure, a location near the MILDEX (Mixed Layer Dynamics Experiment) site, which was familiar to the principal investigators, was chosen.

Since preliminary information could not ensure an ideal, uniform horizontal field with a stable salinity structure and minimal external forcing, the *ex post facto* assessment of site suitability is an important preliminary consideration to any turbulence study that might be undertaken. An examinination of the horizontal thermohaline structure of the site and a study of the balances of heat, salt and momentum in the mixed layer and the upper thermocline is a logical approach to that assessment. The balances of salt and momentum are not considered in this thesis which examines the elements of the heat balance which characterize the upper ocean forcing. It will also determine whether significant horizontal thermohaline structure exists in the upper 120 meters at the site. This study relies primarily upon the isolation and measurement of any significant mesoscale or sub-mesoscale temperature and salinity features. Equally important is the analysis of salinity and temperature profiles to locate and measure intrusive signatures in the upper thermocline.

The overall heat balance equation of Large *et al* (1986) outlines four processes which combine to close the heat balance to an arbitrary depth, D. This system is:

$$\partial_t H(D) = Q_c + R_v(D) - A_v(D) - A_h(D). \qquad (1.1)$$

The L.H.S. of the equation represents the total heat content or

$$H(D) = \rho c_p \int_{-D}^{0} T \, dz \tag{1.2}$$

and the R.H.S. includes: surface heating

$$Q_c = \rho c_p \int_{t_0}^{t} Q_0(t') \, dt' \tag{1.3}$$

vertical diffusion

$$R_v(D) = \rho c_p (w'T')_{-D} \tag{1.4}$$

vertical advection

$$A_v(D) = \rho c_p \int_{-D}^{0} w \, \partial_z T \, dz \tag{1.5}$$

and horizontal advection

$$A_h(D) = \rho c_p \int_{-D}^{0} (V \cdot \nabla T) \, dz. \tag{1.6}$$

For all of the formulations in the above system ρ is the density of seawater, c_p is the specific heat of seawater, and T is the ambient water temperature at depth z at time t_0 to t. Also, the variables, V and w, represent the horizontal and vertical velocity respectively.

It would be desirable to attempt a complete solution of the heat balance equation and perhaps an analagous salt flux system. The primary purpose of this thesis, however, is to analyze the surface forcing, heat content and horizontal structure to determine the extent to which mixing in the PATCHEX domain may be considered to be solely due to vertical shearing processes. These three contributors directly influence the transfer of momentum, salt and heat into the upper thermocline. The

solution of equations 1.4, 1.5 and 1.6 is deferred since a complete closure of the heat budget is not attempted in this thesis. Absolute velocity data available from the R P FLIP and temperature microstructure data from the R V POINT SUR will be employed in a subsequent study to estimate the remaining terms in the heat balance.

Studies such as D'Asaro (1985) show that large scale surface forcing is intrinsically involved in setting up the near-inertial wave climate responsible for the hypothesized shear related mixing. He indicated that storm induced mixing extended 5-10 meters below the mixed layer and was correlated with the phase of near-inertial currents. The total heat content and surface forcing terms are readily calculated and can be usefully compared irrespective of the other terms in the heat balance. These terms affect the temporal evolution of the temperature field and the depth of the seasonal mixed layer and hence, the temperature and momentum fluxes into the upper thermocline which directly affect mixing there.

Horizontal temperature gradients can be estimated due to the spatial nature and high resolution of the R/V POINT SUR measurements. These data, which are described in Chapter II, provide a detailed analysis of the character and the spatial and temporal evolution of the horizontal thermohaline environment. This information is employed to directly determine if significant horizontal temperature gradients exist within the PATCHEX domain which may be related to mesoscale features. In summary, The goals of this thesis are:

- to examine the surface forcing and the heat content elements of the heat budget;
- to map the horizontal temperature structure of the survey area and follow its evolution;
- to relate the evolution of the temperature field to the ambient forcing and the total heat content; and
- to observe the vertical coherence of significant horizontal structures through the mixed layer and into the upper thermocline.

To effectively consider surface forcing, heat content and horizontal temperature structure, the R/V POINT SUR data were analysed and displayed using a variety of methods and formats. Time series of surface forcing and cumulative heating were produced using a full stability corrected algorithm. The total heat content of the mixed layer was determined as a cumulative time series by solving equation 1.2. Horizontal temperature gradients and vertical coherence of those gradients were tracked by examining time series of temperature at constant depths of 10, 40 and 100 meters.

Where those gradients were significant, it was attempted to map them onto a grid of the entire PATCHEX domain with an objective analysis. All of these tools provide valuable information which sets the stage for the microstructure analysis of the PATCHEX data. Only after these areas are developed in conjunction with the detailed oceanographic synopsis which is provided in Chapter IV, can an accurate assessment of shear related mixing be undertaken.

II. DESCRIPTION OF THE EXPERIMENT

A. THE PARTICIPANTS

Although this thesis concerns measurements made by NPS researchers aboard R/V POINT SUR, the concurrent measurements made by the participants in PATCHEX collectively illustrate the spatial characteristics of the site and are described below. The Scripps Institution of Oceanography research platform, FLIP, was the first participant to arrive on station at 34°N 128°W where she was moored for the duration of the experiment. The main instrument suite aboard FLIP consisted of four systems. The first was a pair of Seabird CTD's for profiling to 600 meters every three minutes with 1 meter resolution for temperature and 3 meters for density. Four downward slanting incoherent doppler sonar transducers were mounted at 38 meters depth and oriented 55° down from the horizontal to provide 20 meter resolution velocity shear measurements from 75 to 1000 meters depth. To describe the large scale horizontal velocity field within the mixed layer, two horizontally mounted transducers similar to those employed in the slant array were used. A finer depiction of the near surface velocity field was obtained from a coherent acoustic doppler velocity profiler which measured shear over a 50 meter range to 1 meter resolution.

The next vessel to arrive was the R/V POINT SUR on 3 October. A detailed account of her role is summarized in the next section of this chapter. The R/V THOMPSON from the University of Washington arrived on 4 October to deploy three primary systems. A Richardson Number (RhiNo) neutrally buoyant float equipped with velocity shear and stratification sensors was deployed approximately 4 kilometers from FLIP. A Benthic Acoustic Stress Sensor (BASS) on the float provided 0.03 cm/sec resolution of the velocity field at 5 points over a 5 meter range. The float also carried an array of eight fast response thermistors which were spaced vertically and logarithmically throughout the BASS field to provide fine scale temperature information over the same range. Temperature and velocity microstructure measurements were obtained by the next two systems: an advanced microstructure profiler (AMP) which provided repeated profiles of small scale shear and temperature gradient to a depth of 300 meters and a multi-scale profiler (MSP) which measured shear, temperature and velocity microstructure, and profiler orientation to 1000 meters depth.

The last participant to arrive on scene was the USNS DE STEIGEUR with a team from the Naval Research Laboratory (NRL). The NRL instrumentation consisted primarily of three systems. Their unique contribution to the effort was a towed thermistor chain which resolved 0.5 meter vertical sections of thermal structure. To accomplish this, the chain contained 180 thermistors spaced 0.5 meters apart and 8 conductivity sensors spaced 2.5 meters apart. To provide finer resolution of features discovered by the thermistor chain, NRL also carried a High Resolution Vertical Array (HVR) mounted on a Sea Soar profiler. The HVR contained 30 thermistors spaced 0.1 meters apart and 2 conductivity sensors. An RDI Doppler Current Profiler (DCP) on DE STEIGEUR provided velocity information. Its depth range was 200 meters, vertical resolution 8 meters and velocity resolution 2 cm/s averaged over 1 minute.

B. MEASUREMENTS FROM R/V PT SUR

The R/V POINT SUR departed Monterey, California shortly after noon on 2 October 1986 and arrived to rendevous with R/P FLIP on the evening of 3 October. To provide oceanographic ground truth for the experiments to follow, a 20 kilometer CTD survey was made on 4 October. Eight casts to 1000 meters were made within the survey area using a Neil-Brown Instruments Systems (NBIS) CTD. Shortly thereafter, NPS researchers began conducting a detailed survey of an 8 kilometer square box centered on FLIP. This was accomplished using a procedure known as a toywo. In a towyo survey, a towed instrument package is alternately raised and lowered through the water column while the vessel is underway. This is done to acheive a three dimensional picture from a single sensor package. The towyo was deployed continuously throughout the experiment to gather detailed CTD, microconductivity and finescale shear profiles. Four systems were on the towyo package deployed from the POINT SUR. These systems included:

- a Coherent Acoustic Doppler Velocity Profiler (CADVP) capable of estimating 3-component velocity profiles 5 times per second with 10 centimeter resolution over a 5 meter range. It employs a projector and four receivers as illustrated in Figure 2.1;
- a Cox style microconductivity sensor sampled at 1024 Hz;
- an NBIS CTD sampled at 32 Hz; and
- pitch, roll, heading and 3 axis acceleration sensors.

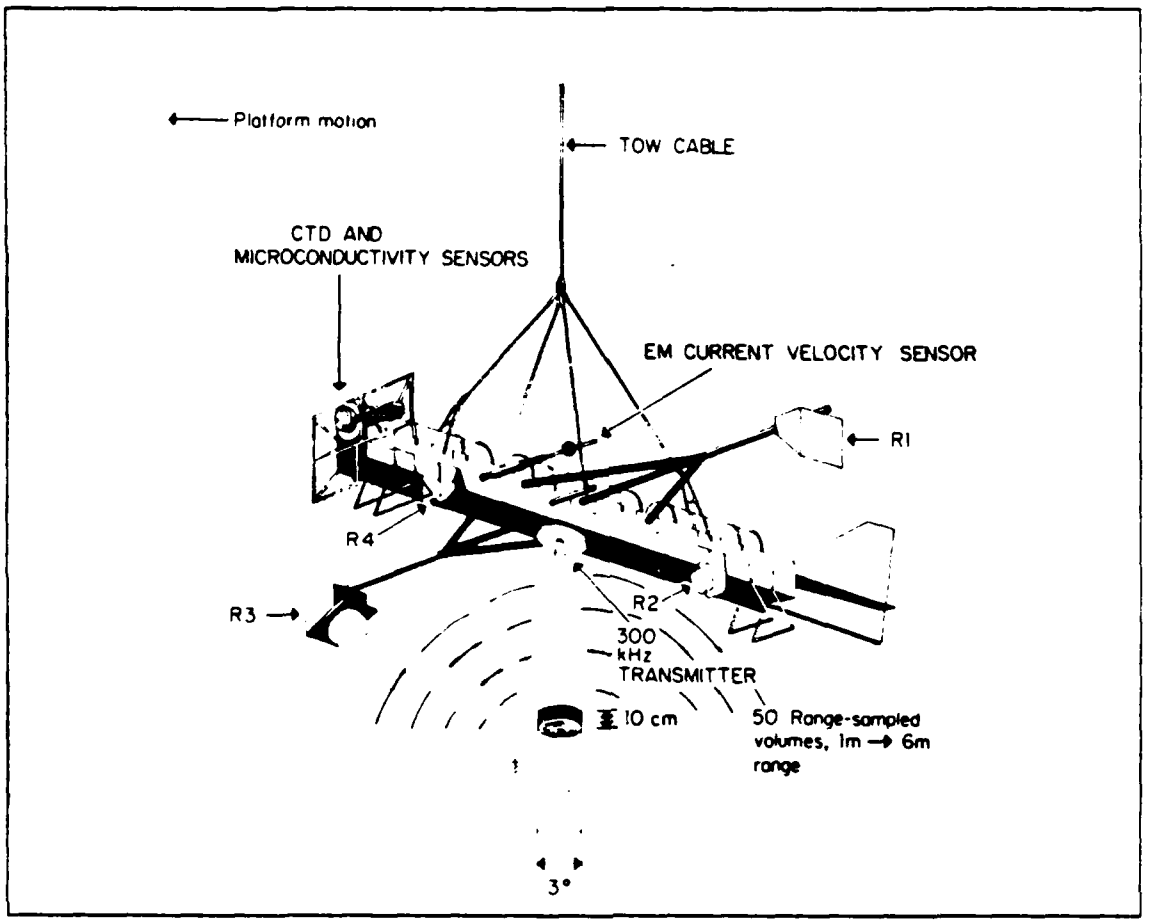

Figure 2.1 R/V Point Sur PATCHEX TOWYO Profiler.

Due to high platform motion the value of the velocity data obtained by the coherent system requires further processing and evaluation to determine its resolution of the finescale shear field. A ship mounted Ametek Straza 4400 Acoustic Doppler Velocity Profiler (ADVP) concurrently obtained velocity profiles. This 300kHz, 4 beam "JANUS" geometry system sampled every 0.6 seconds to provide velocity information to 102 meters depth. Dead reckoning for shipboard navigation was also augmented by the ADVP which provided accurate estimates of the ship's velocity relative to a reference depth current. A Sperry gyro-compass, Magnavox MX-1180 transit satnav receiver, Internav LC408 Loran-C receiver and Motorola Miniranger (providing ranging from FLIP) completed the navigation suite. Thirty second averages of standard meteorological and oceanographic parameters, which are summarized in the next section, were recorded throughout the cruise.

The primary sampling strategy covered a butterfly shaped pattern whose southeasterly and southwesterly diagonals intersected alongside FLIP and whose sides ran in a north-south direction. It was employed to provide a repeated, quasi-synoptic 3 dimensional representation of the velocity and thermohaline character of the upper ocean over an 8 kilometer domain including radial intersections with FLIP. These intersections allow decorrelation scales for both thermohaline and shear features to be determined by intercomparison of concurrent POINT SUR and FLIP measurements.

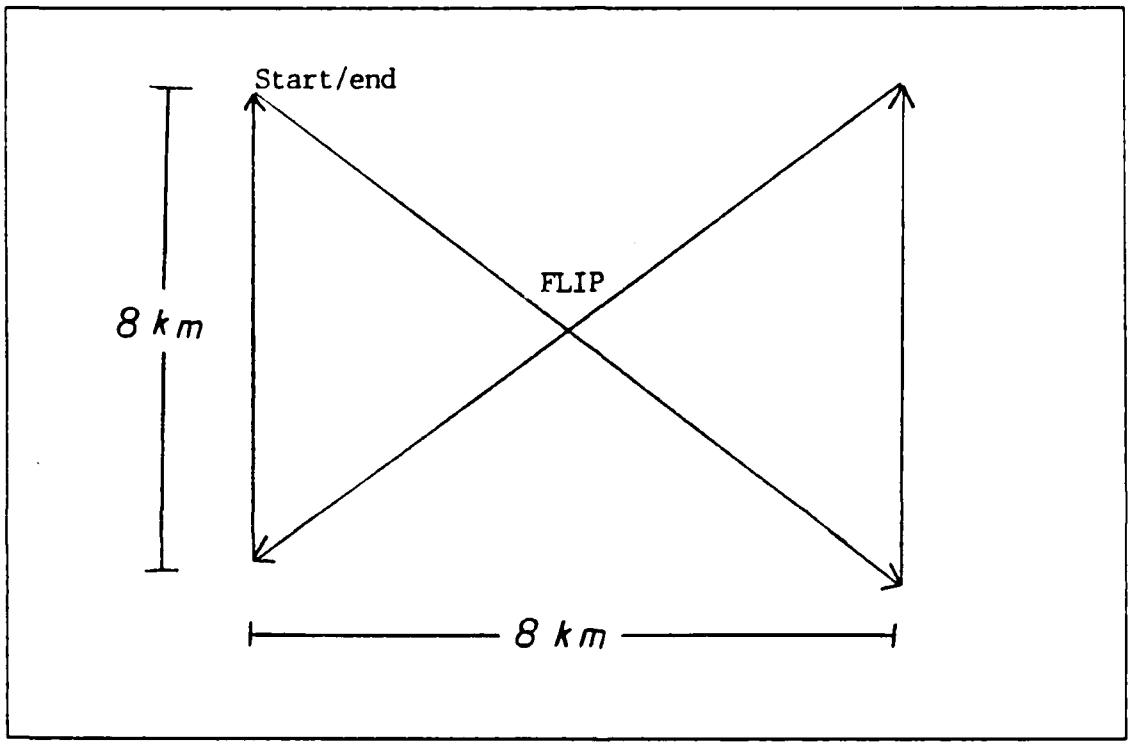

Figure 2.2 PATCHEX Survey Track, 05-13 October.

This geometric pattern which is depicted in Figure 2.2 was continuously surveyed from the beginning of the exercise on 4 October to 13 October. On 13 October, a triangle pattern which eliminated half of the original track was adopted to decrease the cycle time between patterns. Figure 2.3 depicts this pattern which necessarily decreased the coverage area in order to improve the synopticity of the sampling process. Until 13 October, most of the towyo profiles taken were between 5 and 120 meters although deep profiles to 300 meters and 15 meter constant depth runs were also periodically made. After 13 October, nearly all profiles were taken from 100 to 300 meters. During

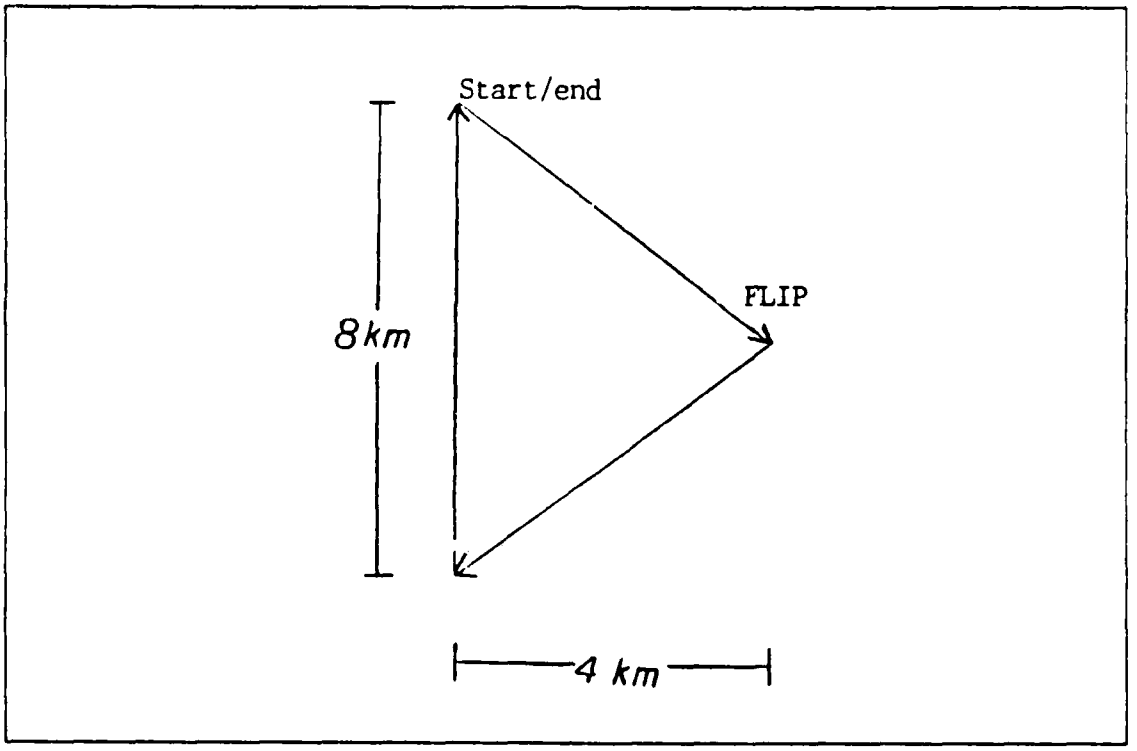

Figure 2.3 PATCHEX Survey Track, 13-16 October.

the latter period, measurements were also taken in a drifting mode for several hours at a time in conjunction with MSP drops from the R/V THOMPSON. Late on 11 October and into 12 October, 3 additional 1000 meter CTD casts were taken along a 20 kilometer diagonal which bisected the PATCHEX domain.

A large scale velocity survey was conducted on 11 October in which 12 expendable current profilers (XCP's) were dropped every 4 kilometers from the POINT SUR along an L-shaped track. These XCP's provide arbitrarily referenced horizontal velocity profiles with 10 meter resolution or better from the surface to 1200 meters. Four of these probes were beyond shelf-life and failed. The results of that survey will be encorporated in future PATCHEX analyses.

C. DATA ACQUISITION AND PROCESSING

The PATCHEX data set was large an diverse. Over 5 gigabytes (billion bytes) of data were recorded on 108, 10 inch, 9 track tapes. To collect and monitor the data stream effectively, an integrated data logging system was developed. Prior field programs by NPS researchers aboard the POINT SUR used the SAIL (Serial ASCII

Instrumentation Loop) Data Acquisition System, or SDAS, to monitor standard shipboard instrumentation. PATCHEX also employed SDAS but modified it to output its data as a synchronized common header to the towyo logging system. The parameters which were recorded by SDAS are listed in Table 1. Towyo data have already been described.

TABLE 1

R/V PT SUR STANDARD INSTRUMENTATION

No.	Data	No.	Data
1.	Year	18.	Pumped Flow Rate
2.	Month and Day	19.	Satnav Degrees Lat.
3.	Hour and Minute	20.	Satnav Minutes Lat.
4.	Second	21.	Satnav Degrees Long.
5.	LORAN Degrees Lat.	22.	Satnav Minutes Long.
6.	LORAN Minutes Lat.	23.	Ship's Heading
7.	LORAN Degrees Long.	24.	Ship's Speed
8.	LORAN Minutes Long.	25.	Time
9.	Dewpoint	26.	Boom SST
10.	Air Temperature	27.	Visible Insolation
11.	Relative Humidity	28.	IR Insolation
12.	Pumped Sea Temperature	29.	IR Pyranometer Temp. 1
13.	Pumped Conductivity	30.	IR Pyranometer Temp. 2
14.	Pumped Salinity	31.	Forward Velocity
15.	Open	32.	Miniranger-A Range
16.	Relative Wind Speed	33.	Miniranger-B Range
17.	Relative Wind Direction		

The data, whose acquisition is summarized in Figure 2.4 were recorded on 10 inch magnetic tape for later processing with a Hewlett-Packard 9020 minicomputer. ADVP data, which had been provided to the towyo logging system by SDAS were fed to the program PAMSUR which produced velocity profiles relative to the ship. PROCCTD processed towyo data that had been acquired simultaneously with SDAS and ran in a seperate partition of the 9020. The program provided spectral corrections to conductivity data from the profiler's NBIS CTD. Given the faster response of the conductivity sensor compared to the thermistor, which had a slower and velocity dependent response, it was possible to provide corrections which ultimately resulted in 6 parts per million resolution in 0.25 meter bins. The final result of this process was that salinity signatures were kept free of spiking to minimize false overturn signatures when density profiles were estimated. To calibrate the microconductivity sensor, CTD conductivity data was high pass filtered and compared with the low passed

microconductivity signal. The processed profile data with corresponding directory information were stored for each profile on a Bering 70 MB hard disk. Figure 2.5 details the steps in the data processing procedure.

Accurate reconstructions of the ship's track, which was dead reckoned relative to FLIP with course, speed and radar positioning underway, was finalized using NAVEDIT, a Basic routine run on the HP-9020. NAVEDIT, which was developed and applied by J. Stockel at NPS, employed all of the navigation information acquired by SDAS. It selected the most applicable and precise data among the variety of navigation information in the data set and tailored each profile's position along a "best track".

The raw physical parameters on hard disk were accessed by OPPROF. OPPROF is a multi-function, post-processing program written in Basic for the HP-9020. It is capable of accessing specified series of profiles and can output graphics and time series of both raw and computed oceanographic parameters. Table 2 is a menu of these outputs. The program can also provide tabular output or a metafile graphics format for

TABLE 2
OPPROF PROCESSING OPTIONS

No.	Data	No.	Data
1.	Temperature	11.	U Shear
2.	Conductivity	12.	V Shear
3.	Salinity	13.	Speed Shear
4.	Sigma T	14.	Buoyancy Frequency
5.	Optical Transmission (n.a)	15.	Gradient Richardson Number
6.	Flourescence (n.a)	16.	T & S Plot
7.	Chi	17.	Chi and Variance Plot
8.	Demeaned U	18.	T S Plot
9.	Demeaned V	19.	Raw U
10.	Demeaned Speed		

plotting on the IBM 370 mainframe at NPS. The entire series of programs for the HP-9020, with the exception of NAVEDIT and some utility routines in OPPROF, were developed and written by T. Stanton at NPS.

SDAS data from the acquisition process outlined in Figure 2.4 reside on both 10 inch tape and 3.5 inch diskette media. The data on the diskettes were downloaded to mass storage volumes for access on the NPS mainframe. Surface forcing time series were then produced on the mainframe with a FORTRAN program, PATFLUX. The stability corrected flux algorithm in PATFLUX is a subroutine written by P. Guest at NPS.

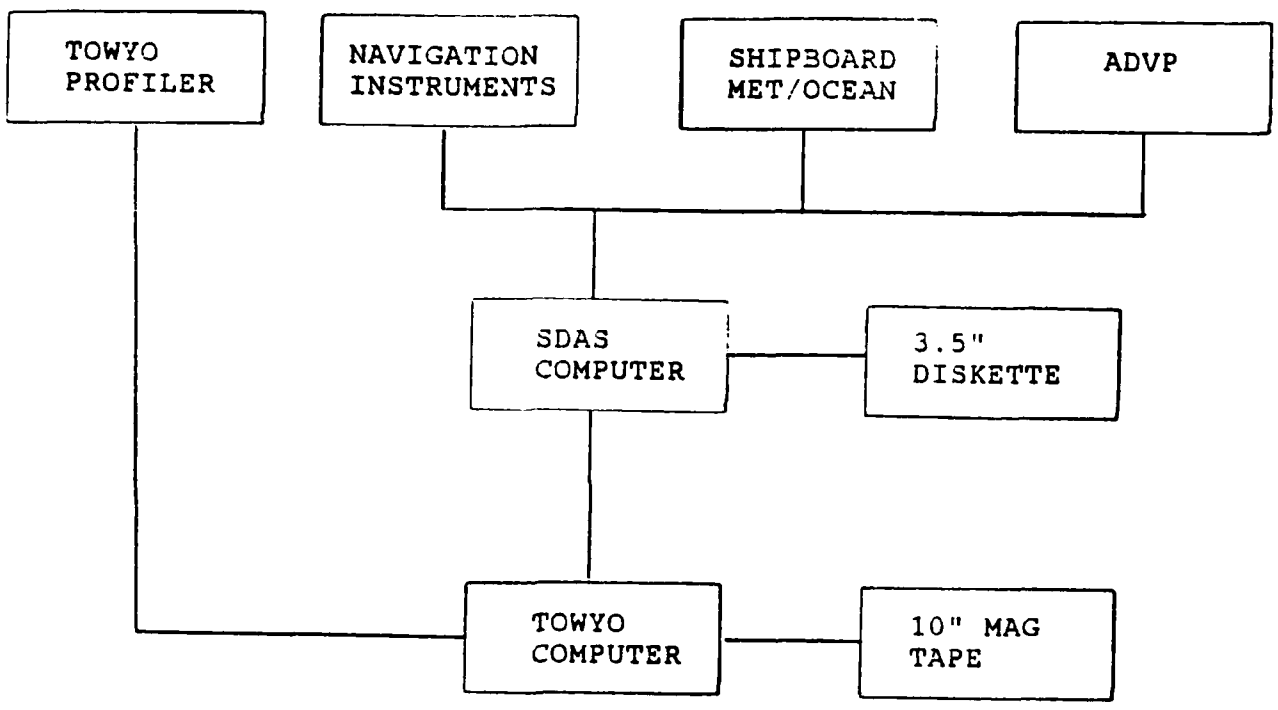

Figure 2.4 PATCHEX Data Acquisition Flowchart.

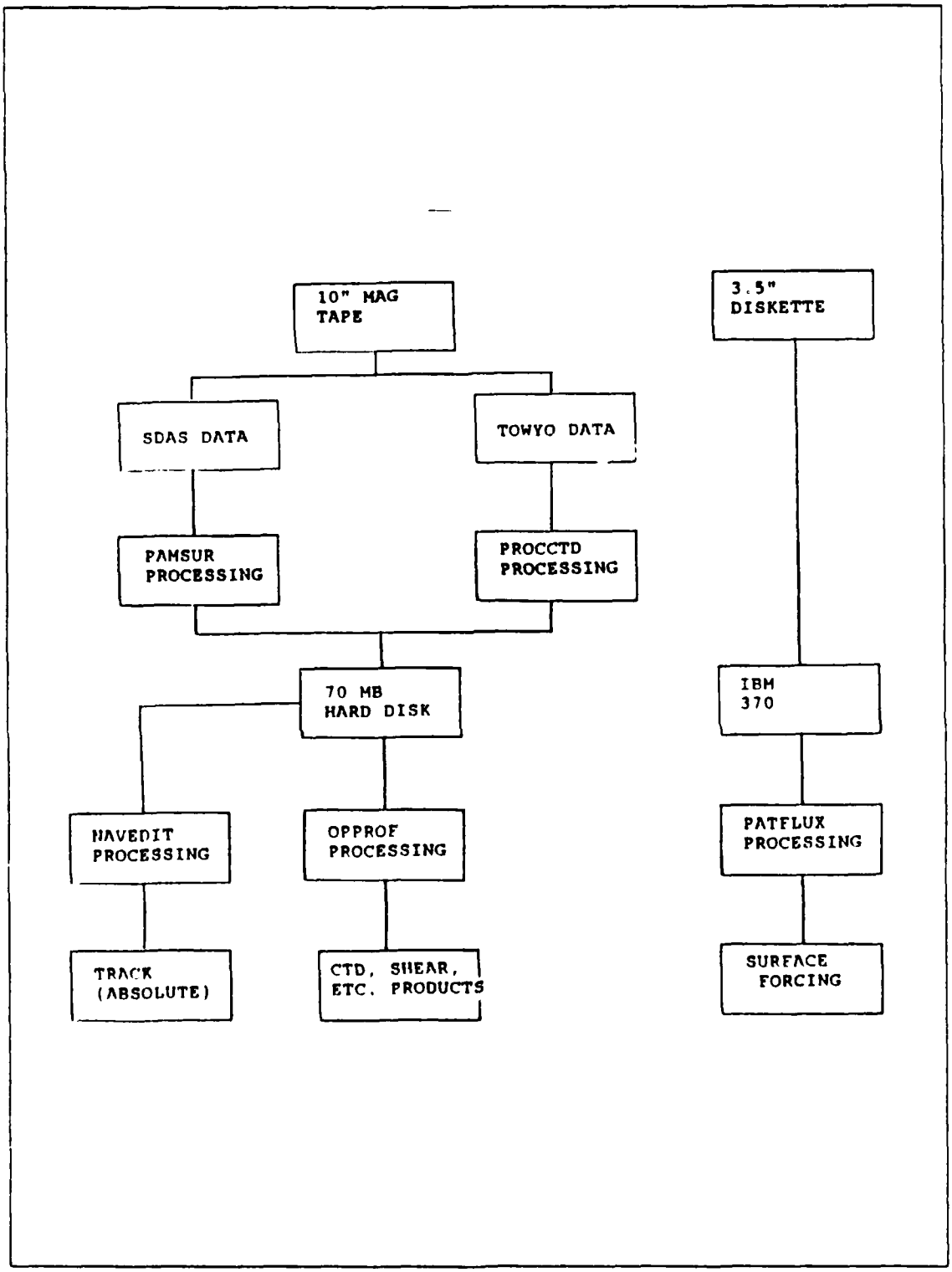

Figure 2.5 PATCHEX Data Processing Flowchart.

III. SURFACE FLUXES

A. SYNOPTIC METEOROLOGICAL SITUATION

Large *et al* (1986) observed that over 63% of the autumnal cooling of the sea surface during the 50 days of STREX (Storm Transfer and Response Experiment) was due to nine 1-2 day storm episodes and only 23% was from radiative forcing and entrainment. Davis et al (1981) had previously observed that the evolution and decay of the mixed layer is also primarily a result of storm activity. Near gale conditions with significant precipitation were noted from 1-3 October, 1986 at the PATCHEX site. Conditions had begun weakening, however, with light intermittent precipitation and clearing when the R/V POINT SUR began surveying the area at 1000 local time on 4 October. By 6 October, fair conditions developed and continued for the rest of the experiment.

The high winds and precipitation observed at the outset of the experiment were not related to a typical transitory cyclone in the mid-latitudes. Rather, they resulted from instabilities associated with the gradient between an intense northeastwardly moving 1034.5 mb subtropical high in the central eastern Pacific near 42N 142W and a strong inverted trough of low pressure whose 1004.8 mb center was located over southern Nevada. The trough extended northeastward through California and Oregon and out to sea as the low center moved slowly eastward and weakened. The evolution of the surface pressure and wind fields at the outset of the PATCHEX experiment is depicted in Figure 3.1 The top panel is the surface synopsis at 011200Z October 1986. It illustrates the 30 knot northerly winds that prevailed at 35N 127W when the R V POINT SUR departed Monterey. These winds persisted at the PATCHEX site (marked by an X in the figure) for over 24 hours then gradually abated as the pressure gradient weakened. The synoptic meteorological situation at 041200Z shortly after the arrival of the R V POINT SUR and 5 hours before she began surveying is depicted in the bottom panel of Figure 3.1. At that time the winds were still northerly but at only 10 knots. The top panel of Figure 3.2 depicts the surface synoptic situation at 060000Z. This is roughly when this thesis begins, with the winds increasing to 16 to 18 knots by 070000Z. These winds persisted for 24 hours then decreased to 10 to 12 knots by 080000Z. This can be seen in the bottom half of Figure 3.2.

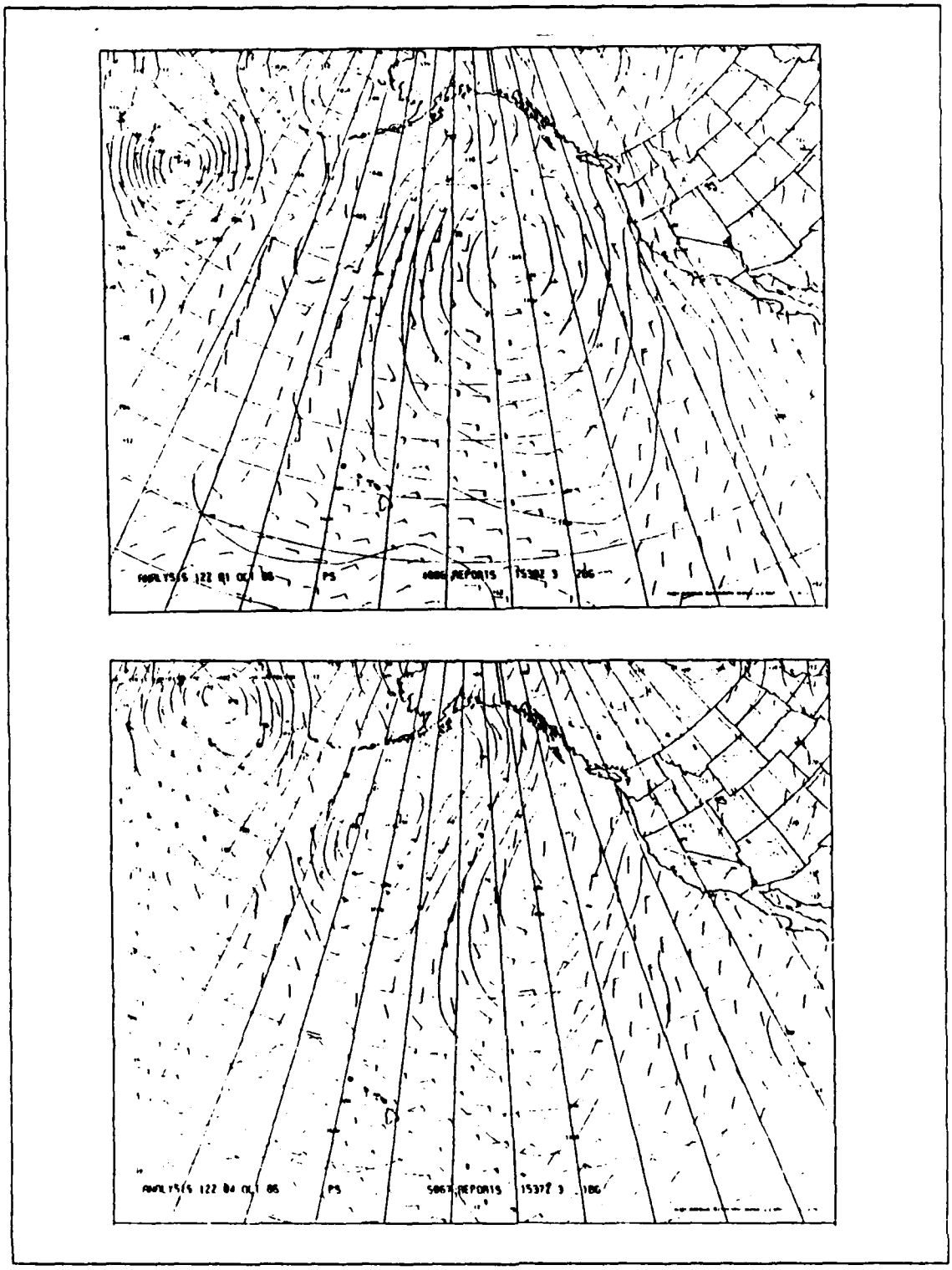

Figure 3.1 01 and 04 October synoptic situation at 12Z.

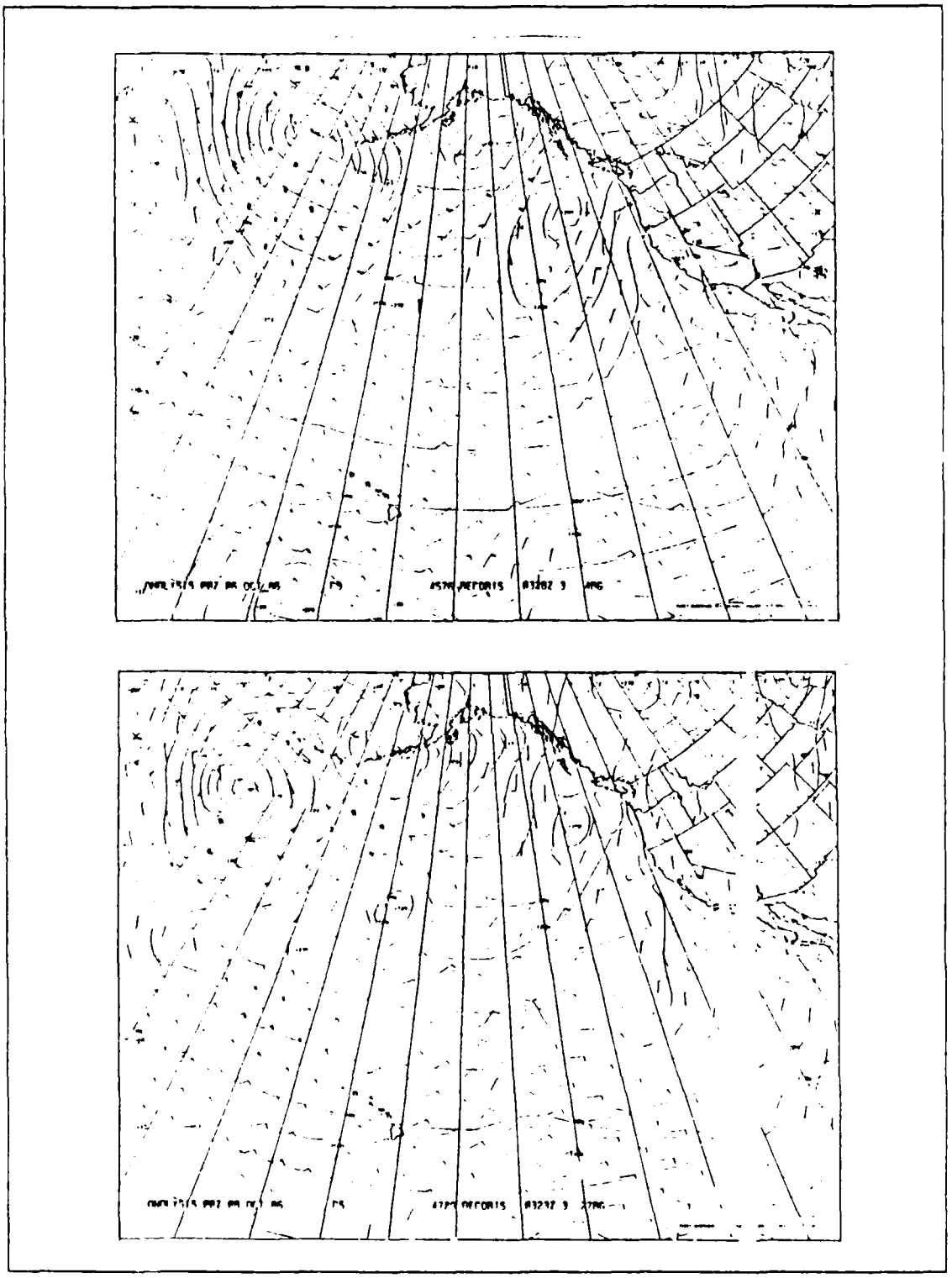

Figure 3.2 06 and 08 October synoptic situation at 00Z.

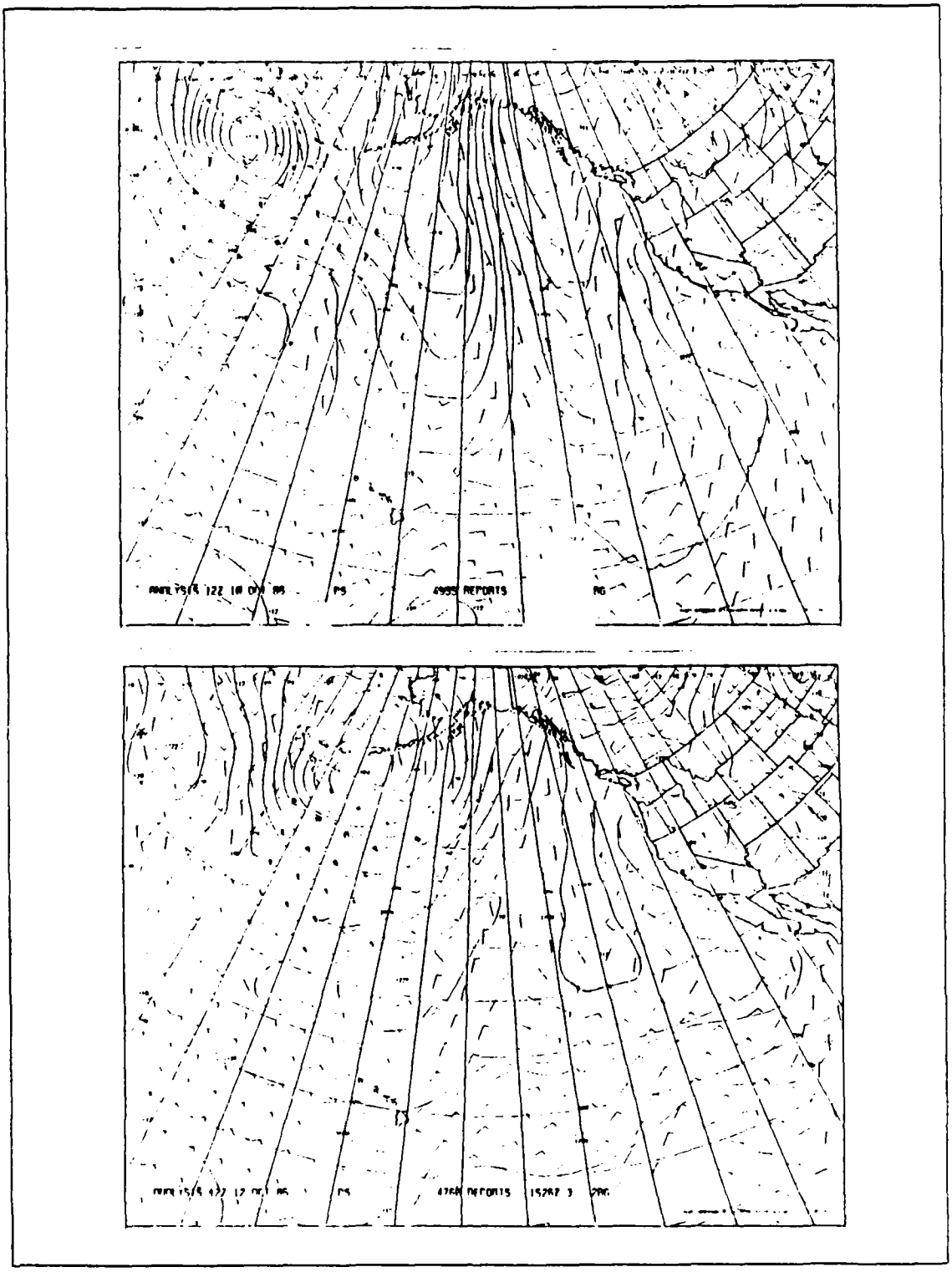

Figure 3.3 10 and 12 October synoptic situation at 12Z.

The wind remained near 12 knots through 9 October and is depicted as such in the 101200Z map, the top panel in Figure 3.3. By 110000Z the wind began to weaken and despite some gustiness at 111200Z, the wind continued decreasing and had become light and variable by 121200Z. The bottom panel of Figure 3.3 illustrates the synoptic situation at this time. Note the strength and extent of the semi-permanent subtropical anticyclone which is the underlying cause of the prevailing conditions. It is the extreme atmospheric subsidence associated with the subtropical high that creates a large dewpoint depression and sets the stage for substantial latent heat release from the ocean surface. Detailed time series of the actual forcing of the marine boundary layer by the transfer of ambient mechanical and thermal energy are explored in the next section.

B. SURFACE FLUX THEORY AND BULK PARAMETERIZATIONS

The ocean is forced by many thermal and mechanical processes. In the absence of precipitation, local wind stress and heat fluxes are the mechanisms primarily responsible for short term variations in the diurnal mixed layer depth and the position of the seasonal thermocline. The rain which was observed prior to the arrival of the R/V POINT SUR had ceased shortly after she began surveying. To determine the atmospheric forcing, continuous measurements of bulk aerodynamic properties were taken onboard the R/V POINT SUR throughout the cruise. Since direct measurement of vertical gradients of velocity, temperature and humidity at scales small enough to infer the fluxes within the surface layer of the atmosphere are generally not attempted at sea, they were estimated by employing Monin-Obukhov similarity theory, which for this development, uses the notation of Panofsky and Dutton (1984).

The small scale gradients in the atmosphere are a function of wind stress, heat flux and surface roughness alone. The effects of thermal and mechanical forcing on turbulence can be combined in theory to produce a scale velocity, u_*, which is the square root of the wind stress (τ) over density (ρ), ie.

$$u_* = \sqrt{\tau \rho} \tag{3.1}$$

and a scale length

$$L = L(u_*, Q_0) \tag{3.21}$$

which is called the "Obukhov" length. In turn, these fundamental quantities may be applied to develop temperature and humidity scales which allow the surface fluxes to be estimated.

Altering the form of our velocity scale expression as stated in equation 3.1 to

$$u_*^2 = \tau/\rho = <-u'w'> \tag{3.3}$$

fundamentally defines the wind stress. Monin-Obukhov scaling also develops a similar temperature flux formulation

$$u_*T_* = <-\theta'w'> \tag{3.4}$$

where θ' the potential temperature, is the temperature that a parcel of air would have if it were displaced adiabatically from its present level to the 1000 mb level. There is also an expression for the specific humidity flux

$$u_*q_* = <-q'w'>. \tag{3.5}$$

A rigorous derivation of the Obukhov length scale is obtained by manipulating the turbulent kinetic energy equation. The solution of a scaling problem, however, is not achevieved explicitly. In practice, the velocity scale is determined first by initially expressing the wind shear as a product of scaling parameters and a "dimensionless shear" such that

$$\partial u/\partial z = \varphi_m u_*/kz \tag{3.6}$$

where $k = 0.4$ is von Karman's constant and φ_m represents the dimensionless wind shear. An accepted convention as expounded by Panofsky and Dutton (1984) states that

$$\varphi_m = 1 - 16\xi, \quad 2 \leq \xi \leq 0 \tag{3.7}$$

under unstable surface conditions, and

$$\varphi_m = 1 - 7\xi, \qquad \xi > 0 \tag{3.8}$$

for the stable case. In these expressions $\xi = z/L$. The constants 16 and 7 continue to be the subject considerable debate and research. Large and Pond (1982), which this study follows, suggests that for the stable case the constant is 7, and not 5, which is a convention used by Panofsky and Dutton (1984). The constant in the unstable case is generally agreed to be 16.

Integrating the expression 3.6 from the surface roughness height (z_0) to the measurement height (z) produces the diabatic profile relation

$$u_* = ku \{ \ln(z/z_0) - \psi_m(\xi) \} \tag{3.9}$$

in which $\psi_m(\xi)$ can be approximated for the unstable case with the formula of Paulson (1970)

$$\psi_m = \ln \{(1+X^2)/2 + ((1+X)/2)^2\} - 2 \operatorname{atan} X + \pi/2, \tag{3.10}$$

where the variable, X, is defined as

$$X = \sqrt{(1 - 16\xi)}. \tag{3.11}$$

For the stable case, a much simpler relation exists, *i.e.*

$$\psi_m = -7\xi. \tag{3.12}$$

Three methods are commonly used to evaluate scaling arguements. These include the eddy correlation method, the dissipation method and the bulk aerodynamic method which is employed in this study. Since $\varphi_m = \varphi_m(\xi)$, as noted in equation 3.7 and ξ cannot be found explicitly, an iterative technique is used to refine its value while solving equation 3.9 for u_*. The process begins with an initial determination of the roughness scale (z_0) using a neutral drag coefficient, CDN_{10}, *i.e.*

$$z_0 = z \exp(-k/\sqrt{CDN_{10}}). \tag{3.13}$$

The drag coefficient of Large and Pond (1982) is used. It is a wind dependent quantity whose form in lighter winds is

$$CDN_{10} = 1.14 \times 10^{-3}, \quad U < 10 \text{ m/s}. \tag{3.14}$$

In heavier winds equation 3.14 becomes

$$CDN_{10} = (0.49 + 0.065U) \times 10^{-3}, \quad 10 < U < 25 \text{ m/s}. \tag{3.15}$$

Applying the method of Large and Pond (1982) PATFLUX performs an iterative procedure on T_* and Q_* to provide a stability correction for ξ. Iteration stops when the algorithm fails to improve u_* by more than 5%. The wind stress, or momentum flux was obtained by applying equations 3.9 and 3.3. The net radiative flux is defined as

$$Q_0 = (1-\alpha)Q_S + Q_L - Q_B - (Q_E + Q_H) \tag{3.16}$$

where α represents the albedo or average reflectivity of the ocean surface estimated at 15% for the PATCHEX cruise. This value is based on a graphic global summary of albedo contained in Gill (1982). Q_S and Q_L, incident solar visible and longwave radiation were measured by two shipboard pyranometers. These instruments were mounted on gimballs atop the bridge cabin to ensure that the sensors continuously looked overhead. Infa-red radiation emitted from the sea was estimated using Stephan's radiation law for black bodies

$$Q_B = \varepsilon\sigma T_s^4 \tag{3.17}$$

where the emissivity, $\varepsilon = 1.0$, to properly account for reflected longwave (Large et.al., 1986). Stephan's constant or $\sigma = 5.67 \times 10_{-8}$ W m^{-2} K^{-4}. T_s is the sea surface temperature or SST. The evaporative or latent heat flux was evaluated from the expression

$$Q_E = -\rho L_e u_* Q_*. \tag{3.18}$$

Sensible heating was determined using

$$Q_{H} = -\rho c_{p} u_{*} T_{*}. \tag{3.19}$$

In equations 3.18 and 3.19, ρ is the density of seawater. The temperature is expressed in absolute degrees, *i.e.*

$$T(^{\circ}K) = T(^{\circ}C) + 273.15. \tag{3.20}$$

C. ESTIMATING THE FLUXES

Accurate measurement of the meteorological and radiative forcing at sea is particularly challenging. The heat production and storage, stability, and motion of the platform all contribute to this difficulty. Monin-Obukhov scaling, the standard approach to providing flux estimates, is very sensitive to errors in the four primary input parameters: air temperature, dew point, sea surface temperature and wind speed. The more extreme criticisms of current application of scaling considerations, such as Blanc (1987), belabor worse case senarios where measurement errors produce flux errors approaching 2 to 3 orders of magnitude. However, until there is quantum change in our understanding of air-sea interactions and in the technology employed at the air-sea interface, the present approach provides one of the soundest estimates of the fluxes of heat and moisture (Davidson, personal communication).

The flux of latent heat from the sea surface is best determined by measuring the surface temperature in situ or by direct pyranometric measurement. Both methods have their advantages and drawbacks. It is difficult to measure the skin temperature in situ without penetrating the interface. On the other hand, pyronometeric readings also contain longwave energy from the sun and clouds which is reflected off the sea surface. Pyranometric SST measurements were not employed in PATCHEX. The R V POINT SUR's stern boom trailed a floating platinum resistance thermometer having a 0.001 °C overall temperature resolution. It was expected to provide the most accurate SST measurements. Pumped seawater from several meters below the water line was also measured in an onboard sea chest to effectively provide a "bucket temperature" as a back-up to the boom temperature. Both of the measurements described are superior to engine injection temperatures used in some older studies, which fail to reflect the true SST due to heat contamination from the engine room and due to the subsurface depth of the intake.

It was essential to employ the boom SST data because of the surface stratification which existed after the period of precipitation and during intense daytime solar heating. The preliminary audit of the data set had determined that the difference between the boom temperarure and the CTD temperature was relatively constant and reflected an offset in the boom measurements. Both types of POINT SUR's SST measurements were compared against towyo temperature measurements in the upper 5 meters of the ocean during convective periods when the entire mixed layer was

TABLE 3
SST MEASUREMENT DIFFERENCES, 8 OCTOBER, 3-5 AM

	06 Oct	08 Oct	10 Oct	12 Oct
Seachest	0.077	0.075	0.040	0.032
Boom	0.208	0.161	0.157	0.162

Mean ΔT: Seachest 0.055 Boom 0.172

isothermal. Table 3 is a summary of the differences between the SST and CTD measurements from approximately 3-5 AM local time on 6, 8, 10 and 12 October. The boom temperature difference is approximately 3 times the magnitude of the sea chest difference. Figure 3.4 details the range of temperature differences that were observed for the two sensors. Those ranges are 0.024 and 0.026 for the boom and seachest respectively. The result of the towyo comparison determined an offset to be applied to the time series of the boom SST of -0.172 °C.

Air temperature and wind speed data were not corrected, though the dewpoint was estimated from psychrometer readings for a 24 hour period while the dewpoint sensor was down. The raw forcing data were then used to produce time series of the forcing, the fluxes and the cumulative fluxes for the study. Hourly averages of the meteorological forcing are summarized for the entire cruise in Figure 3.5. This thesis covers Julian days 279 through 285 which is the period from 6-12 October 1986.

A general description of the winds was provided in the first section of this chapter. The detailed time series shows that although there was some variability, the wind was generally fresh and remained between 6-8 m/s for most of this study. This was a critical factor in the maintenance of daytime convection throughout the oceanic

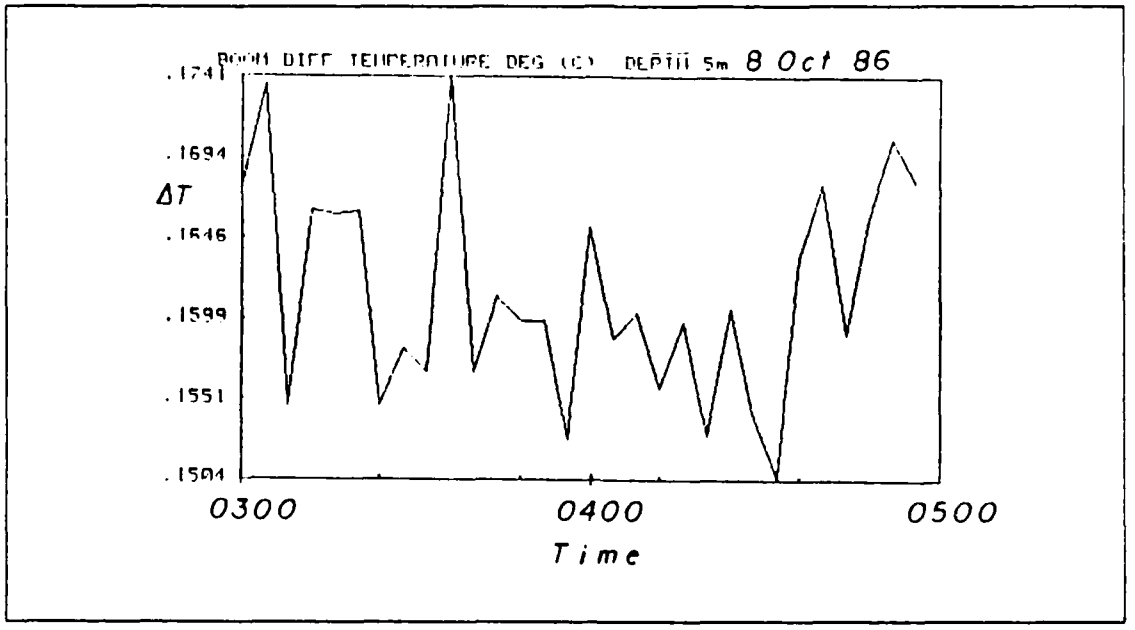

Figure 3.4 SST Measurement Differences.

fossil mixed layer. Toward the end of the experiment, as subsidence associated with the prevailing high pressure peaks, the time series evidences a sharp decrease in the wind. A steadily increasing dewpoint depression can be seen in the time series of hourly mean air temperature and dewpoint. By the end of the study period, it had reached 8°C. Liaison with FLIP (Pinkel, personal communication) confirmed that less than 50% relative humidity persisted over the last half of our measurement period. A peak in SST occurred on October 6 and is depicted in the timeseries of boom and sea chest sea surface temperature. The peak corresponds to the period of maximum surface rainfall accumulation. Note that on previous days, night-time convection had mixed the surface water with the seasonal mixed layer. By the end of 6 October, this mixing had erased all evidence of a surface layer. Smaller maxima in SST and a gradual cooling trend were then observed in the remainder of the timeseries.

The combination of low relative humidity and moderate winds removed a large amount of heat from the sea surface. Although the mean SST depicted in Figure 3.5 only reflects a 0.2-0.3 °C change from the evening of 6 October through the end of 12 October, this represents a significant heat release. Figure 3.6 is a timeseries of the heat and momentum fluxes for the duration of the PATCHEX cruise. Since our period of interest is from Julian day 279 to 286, note the timeseries of latent and sensible heat

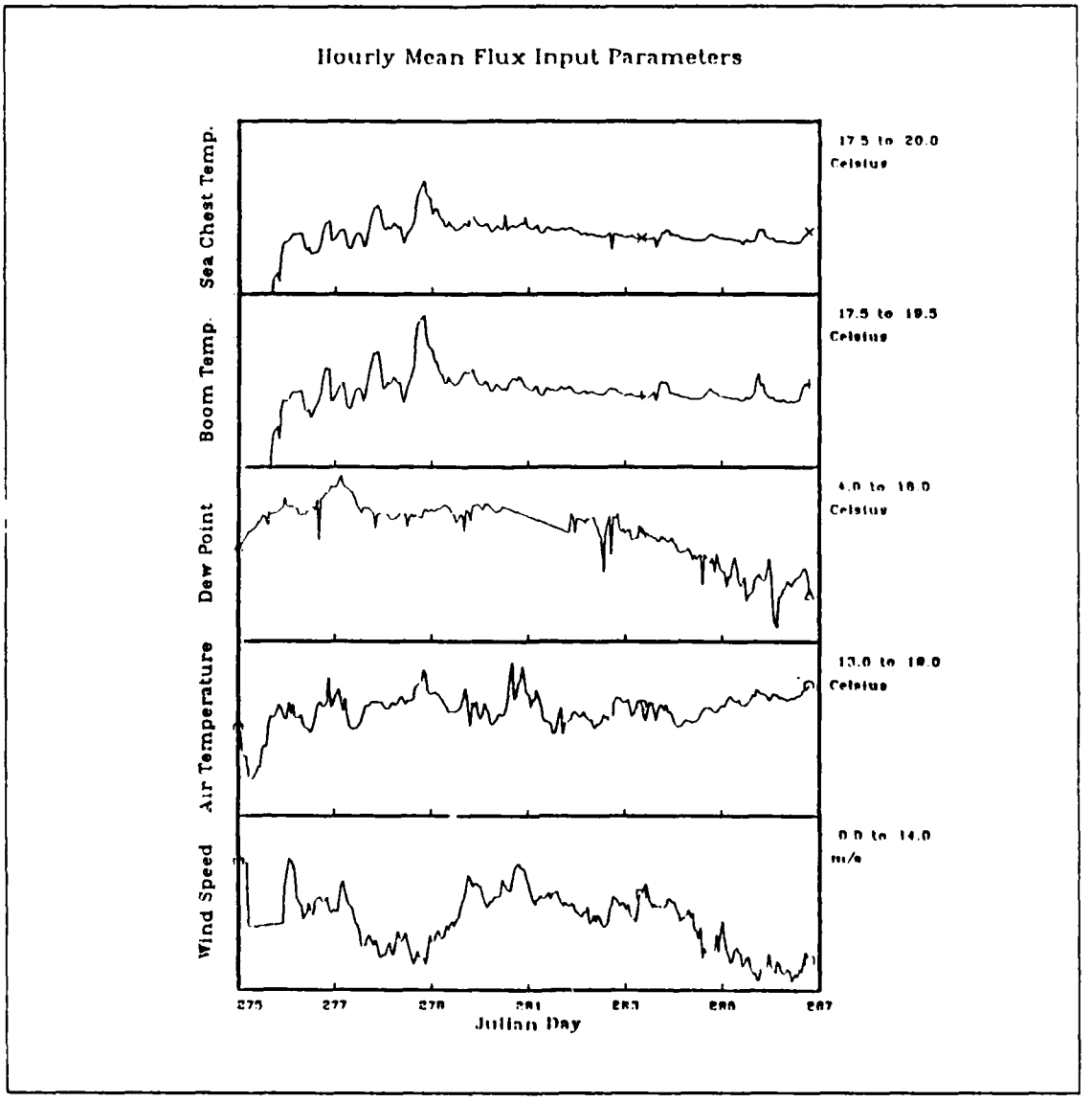

Figure 3.5 PATCHEX Meteorological Forcing.

loss depicted in the two bottom panels of Figure 3.6. Two peaks of 125 W/m^2 of latent heat release can be seen. These maxima occurred in conjunction with increased wind stress episodes on 6 and 7 October. The mean latent heat loss until 11 October was approximately 100 W/m^2. Corresponding sensible heat losses on the order of 75 W/m^2 can be seen in the timeseries. The winds began to decrease on Julian day 285, or 12 October and by day 286 sensible and latent heat loss had dropped to 50 W/m^2 and 20 W/m^2 respectively.

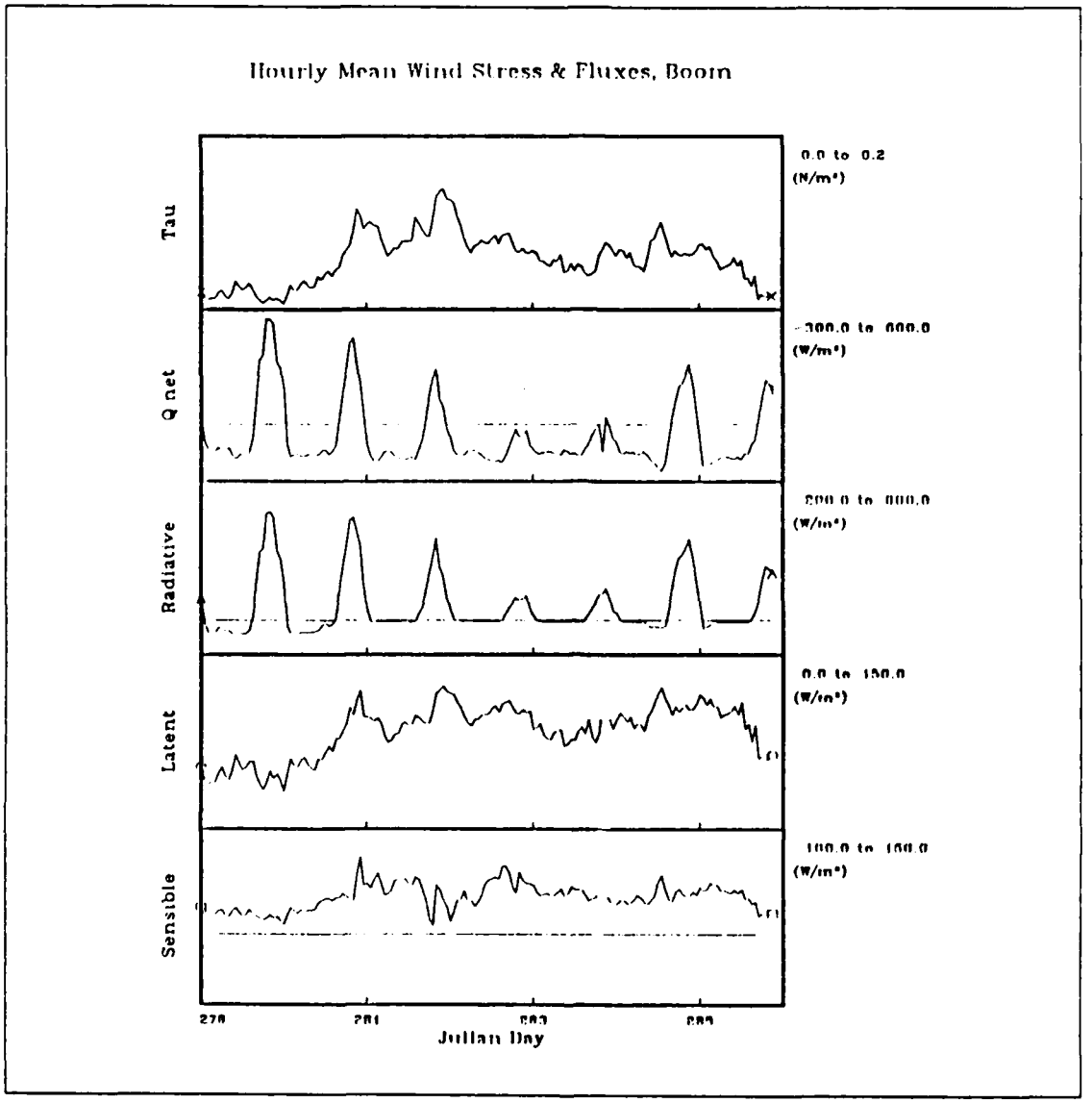

Figure 3.6 PATCHEX Surface Fluxes.

Combined solar longwave and shortwave energy, minus the output of longwave energy from the sea surface, is depicted in the third panel of Figure 3.6. The typical diurnal cycle shown ranged from approximately -200 W/m^2 overnight to 500-700 W/m^2 during peak daytime heating periods. This cycle was interrupted on 9 and 10 October when cloudy conditions limited insolation. In the next chapter, we shall observe that this period of retarded surface heating was instrumental in sustaining and intensifying the cooling within the seasonal mixed layer which erased all traces of a surface layer

(even during the day). The time series of net flux, Q_0, depicts the overall heating and cooling which was estimated at the air-sea interface. It is clear that solar radiation is the largest contributor during the daytime. It should be noted that night-time losses of net heat were increased 3 or 4 times due to the effects of sensible and latent heating after 8 October (Julian day 281).

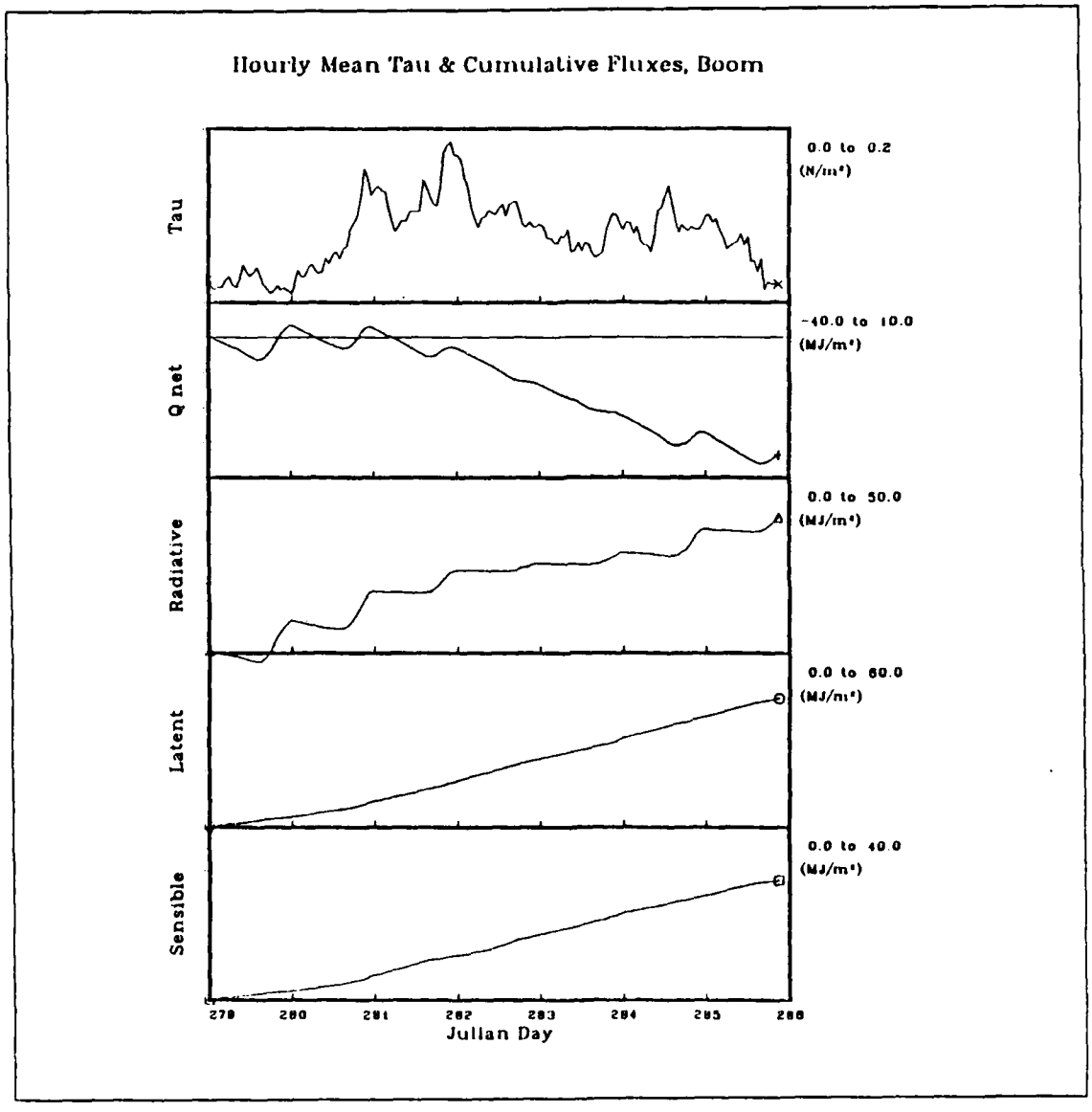

Figure 3.7 PATCHEX Integrated Surface Fluxes.

The surface fluxes were integrated for the study period for later comparison with the total heat content of the fossil mixed layer. Along with the hourly mean wind stress, these quantities are shown in Figure 3.7. Following a ± 5 MJ m^2 diurnal cycle through 8 October a -35 MJ m^2 change in the net flux is observed through 11 October. This is followed by a net increase of approximately 5 MJ m^2 on 12 October. The wind stress and sensible fluxes associated with the subtropical anticyclone were clearly insufficient compensation for decreased insolation and continued latent heat release. The cumulative time series for Julian day 286 through 287 depict additional heating but are not included in this study.

D. ERROR ANALYSIS OF THE SURFACE FLUXES

The accuracies of the various instruments used to measure raw flux parameters are listed in Table 4. They are based upon pre-cruise calibrations for the pyranometers

TABLE 4
ACCURACY OF FLUX SENSORS

Sensor	Accuracy
Air Temperature	0.2 °C
Dew Point Temperature	0.2 °C
Sea Surface Temperature	0.01 °C
Wind Speed	1 m s
IR Pyranometer	1%
Visible Pyroheliometer	0.5%

and both pre-cruise and post cruise calibrations for the temperature sensors. The windspeed error is based upon the anemometer specifications from the manufacturer. The values in Table 4 were employed along with environmental considerations and an audit of the time series of raw parameters to estimate the errors listed in Table 5.

The 30 second average values, recorded by SDAS, provided some smoothing of the raw data from the sensors. For example, although the time series of wind stress appeared noisier during the first days of the experiment, the variability was within range of the ambient environmental conditions and not attributable to instrument error. Low sea state also minimized pitch and roll pumping effects on the anemometer. The error in τ is based solely on instrument error as a percentage of the total wind stress.

Along with the wind stress, Table 5 also contains 1 percent error for the fluxes of incoming and outgoing longwave energy. Incoming solar infared energy error was based upon the 1 percent pre-cruise calibration of the pyranometer. Surface emissivity or back infared radiation, was determined strictly as a function of the sea surface temperature where the boom was recalibrated to within 0.1 °C following the cruise. Incident shortwave solar energy error was estimated at 2 percent, combining the 0.5 percent advertised error of the pyroheliometer with an estimate of the effect of mast shadowing. This effect was estimated as a percentage of outliers in the time series of visible solar flux during clear sky conditions.

TABLE 5
ACCURACY OF SURFACE FLUX ESTIMATES

Flux	Percent Error
τ	2%
Q_B	1%
Q_L	1%
Q_H	3%
Q_S	2%
Q_E	5%
Q_0	14%

Sensible heat flux was estimated based upon the combined effects of the error in air temperature, SST and wind stress as a percentage of the total effect. This accounted for 3 percent error. The largest error term, Q_E, the latent heat, had the addition of the dewpoint error which raised its error to 5 percent. The total error of all the fluxes when combined is 14 percent. This equates to a cumulative flux error of ± 5 MJ m^2 for the 35 MJ m^2 which was lost at the sea surface during this study.

IV. OCEANOGRAPHIC SYNOPSIS

A. VERTICAL CHARACTER OF THE PATCHEX SITE

Chapter II described the spatial and temporal nature of the R/V POINT SUR measurements which allow the thermohaline character of the mixed layer and the upper thermocline of PATCHEX site to be determined. This high resolution dataset provides a detailed oceanographic context for the pursuit of the goals of this study and for the analysis of the microstructure and internal wave measurements made by all of the participants in PATCHEX. In this study, the decision to explore the different areas described in Chapter I was based directly on an analysis of the thermohaline environment. The first phase of that analysis concentrated on the evolution of salinity and temperature profiles within the seasonal mixed layer from 6-12 October 1986.

The preliminary analysis first shows that from 6-8 October the mixed layer was undergoing incomplete daytime mixing due to precipitative stratification and weak surface fluxes. Convective mixing of the entire layer was observed through the night by the absence of jumps in temperature and salinity to the resolution of the CTD (0.001°C and 0.2 millisiemens respectively). Figure 4.1 illustrates typical daytime salinity and temperature profiles observed during the first two days of this study. Temperature steps where $\Delta T < 0.05$°C was observed generally coincided with an active mixing layer. These data were not, however, as sensitive a test for well mixed conditions as was the salinity signature. To determine whether or not thorough mixing existed, salinity was used as the primary tracer. A survey of all of the profiles in the experiment indicate that if $\Delta S < 0.04$ parts per thousand, the entire seasonal mixed layer was overturning.

The salinity signature clearly indicates that active mixing is limited to the region above 10 meters in Figure 4.1. Typically these salinity ledges ranged from 10 to 35 meters in depth during the day. To ensure that salinity features such as that seen in Figure 4.1 are not dismised as sampling artifacts, it is reiterated that 0.5 meter vertical salinity resolution of 0.003 parts per thousand was obtained in the pre-processing phase. It should be noted that these salinity jumps were frequently horizontally coherent features which persisted from profile to profile throughout the domain over time scales spanning several hours. Salinity ledges such as the ΔS of 0.06 ppt near 10

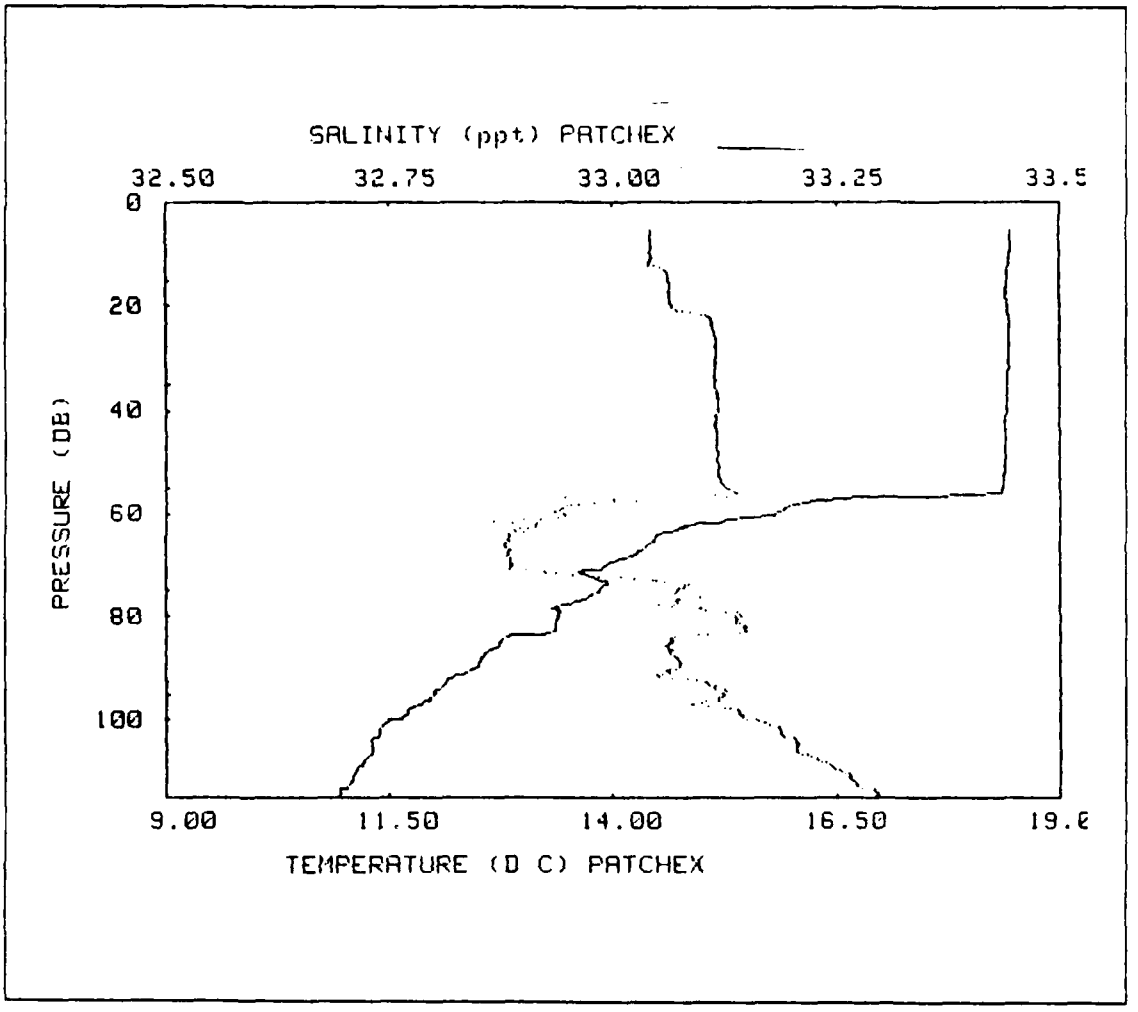

Figure 4.1 PATCHEX Daytime Salinity and Temperature, 6 October.

meters in Figure 4.1 were present during periods of strong surface heating. Otherwise, the step was generally observed near 25-35 meters combined with the ΔS normally seen at that depth (0.03ppt at 35 meters in the example) forming a single, stronger step at the deeper depth. It was common to observe completely active surface layers with a single ΔS as high as 0.16 ppt near 25-35 meters. These events occurred sporadically throughout the day in conjunction with the tenuous balance that existed with the overall forcing. An active daytime surface layer such as this was not observed after 8 October when mixing from wind stress and strong latent heat loss kept entire layer well mixed. As seen in Chapter III, the wind stress quickly peaked on 8 October with corresponding sensible and latent heat losses to begin re-mixing the stratified surface

layer into the fossil mixed layer below. After 8 October, the mixed layer continuously exhibited an isothermal and isohaline character.

The average depth of the base of the mixed layer ranged from 48 to 62 meters. The effects of internal waves were clearly a dominant mechanism in the vertical displacement of the base. Figure 4.2 depicts a typical Brunt-Vaisala profile from the experiment. The large stability signature characteristic of the uppermost boundary of the thermocline illustrates the favorable climate for internal wave activity there due to

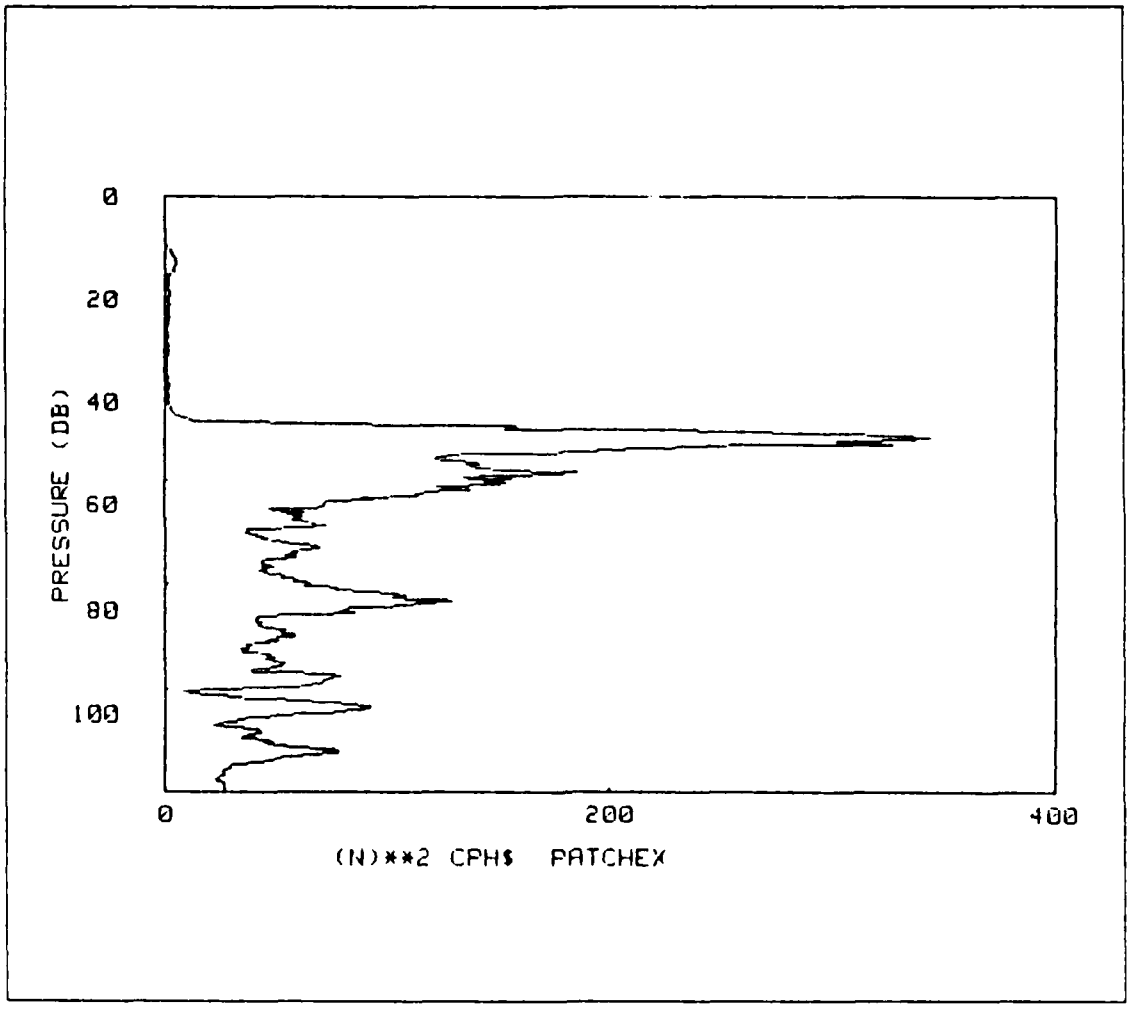

Figure 4.2 PATCHEX Buoyancy Profile, 6 October.

the very strong stratification. Figure 4.3 is a time series of the depth of temperature isotherms for 12, 13, 14 and 16°C, based on averages of every twenty profiles from 6-12 October. The average elapsed time between each profile was between 6 to 9

minutes. The crude low-pass filter produced by the averaging of profiles removes the noisy higher frequencies with periods less than 3 hours and shows the underlying near-inertial or semi-diurnal periodicity by inspection. Consecutive semi-diurnal and inertial

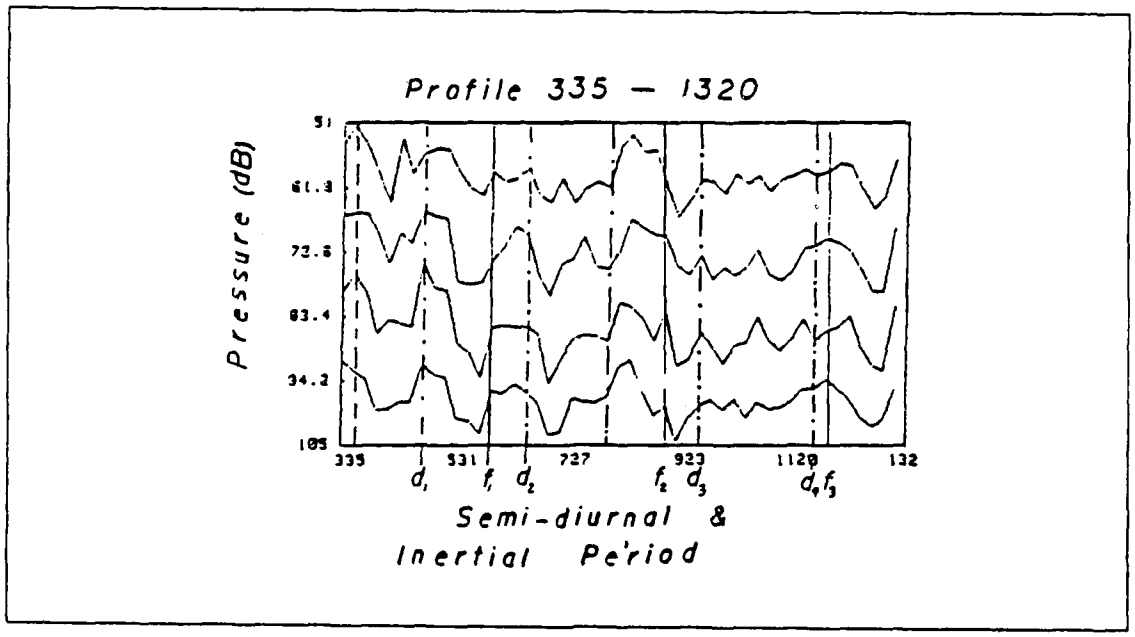

Figure 4.3 12, 13, 14 and 16°C Isotherms, 6-12 October.

periods are denoted in Figure 4.3 by the symbols d_n and f_n respectively. The inertial period at the PATCHEX latitude is 20.84 hours. Dashed lines represent consecutive 20.84 hour increments while alternating dashes and dots represent consecutive 12 hour increments. Inspection of the time series appears to indicate that neither an inertial nor semi-diurnal period dominates the upper thermocline from approximately 50 to 100 meters during this study. For the purpose of this thesis, it is important to establish that below the mixed layer, temporal variations may overshadow the spatial variations that are investigated in the next section. The effect of internal waves is also reflected in the deeper, slightly stratified areas of the mixed layer which appears to contain less horizontal coherence.

To properly characterize conditions within the mixed layer, the complex thermohaline structure in the active upper thermocline cannot be ignored. The activity near the top of the thermocline during PATCHEX is illustrated in Figures 4.4 through 4.7 at the end of this section. Temperature inversions on the order of 0.5°C, as seen in Figure 4.4, were common directly below the base of the mixed layer. These inversions

occurred throughout the study and were often as strong as 1°C. Figure 4.5 depicts the Brunt-Vaisala frequency for the same profile emphasizing the strong stratification which exists in the upper thermocline. Figure 4.6, a velocity profile based on the relative velocity information obtained by the Amatek Straza doppler system depicts a 15 cm/sec speed maximum at the depth of the intrusion noted in Figure 4.4. The degree of active mixing which is occurring is illustrated in Figure 4.7. χ, the temperature variance dissipation rate is defined as

$$\chi = 2D < \nabla_z T' >, \qquad (4.1)$$

where D is the molecular diffusivity of seawater. The maximum in the log of χ associated with the intrusion at 58 meters indicates an increase in active mixing of nearly 4 orders of magnitude near the top of the thermocline as compared to the fossil mixed layer. As noted earlier, signatures such as those in Figures 4.4 through 4.7 were sporadic, though common, and were often sustained for long periods of time. The coincidence of the high χ layer and the salinity-compensating temperature inversions suggests that diffusive processes are dominating the mixing at these depths. This mixing activity will be examined in later studies which emphasize turbulent mixing in the upper thermocline.

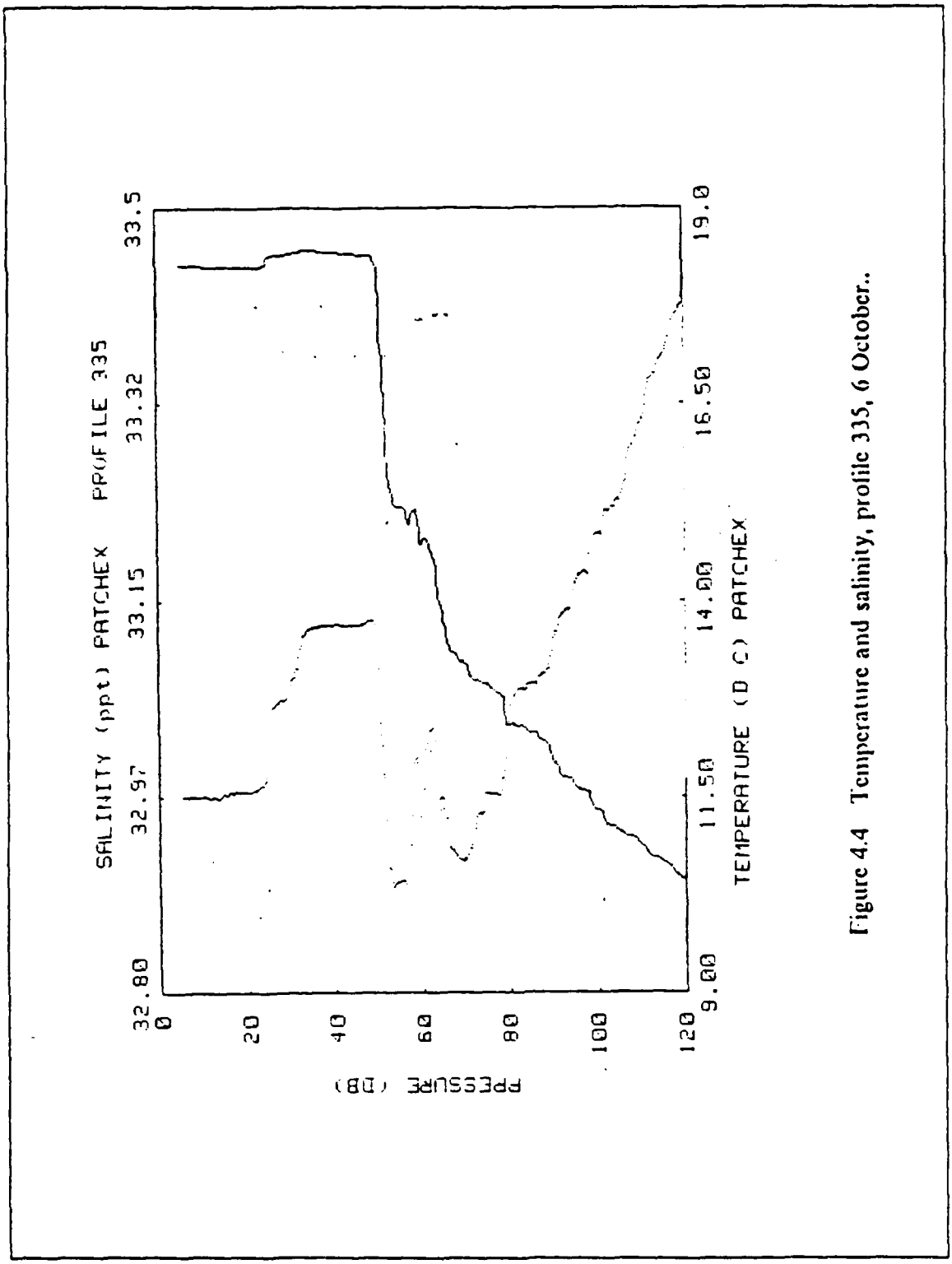

Figure 4.4 Temperature and salinity, profile 335, 6 October..

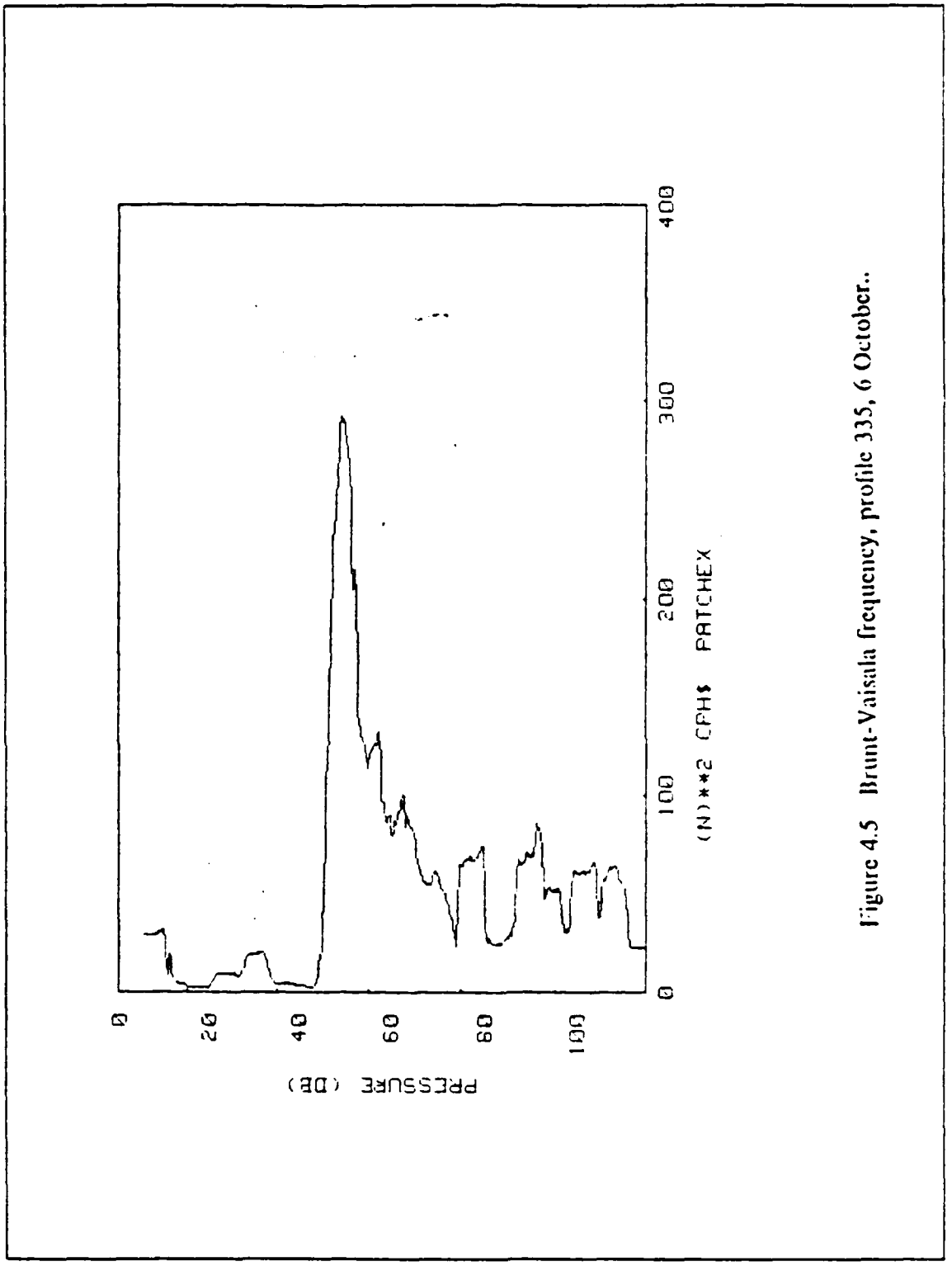

Figure 4.5 Brunt-Vaisala frequency, profile 335, 6 October..

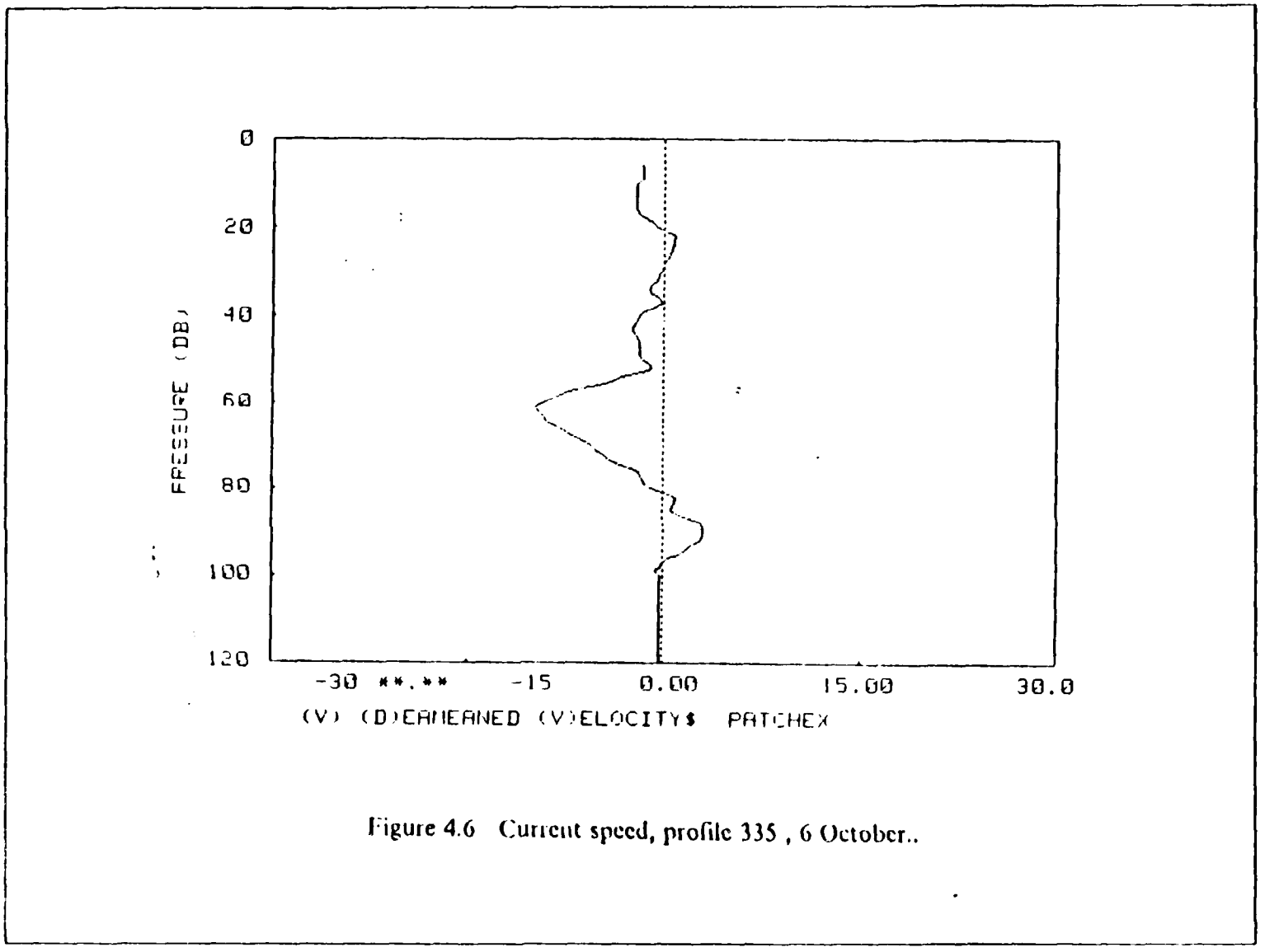

Figure 4.6 Current speed, profile 335 , 6 October..

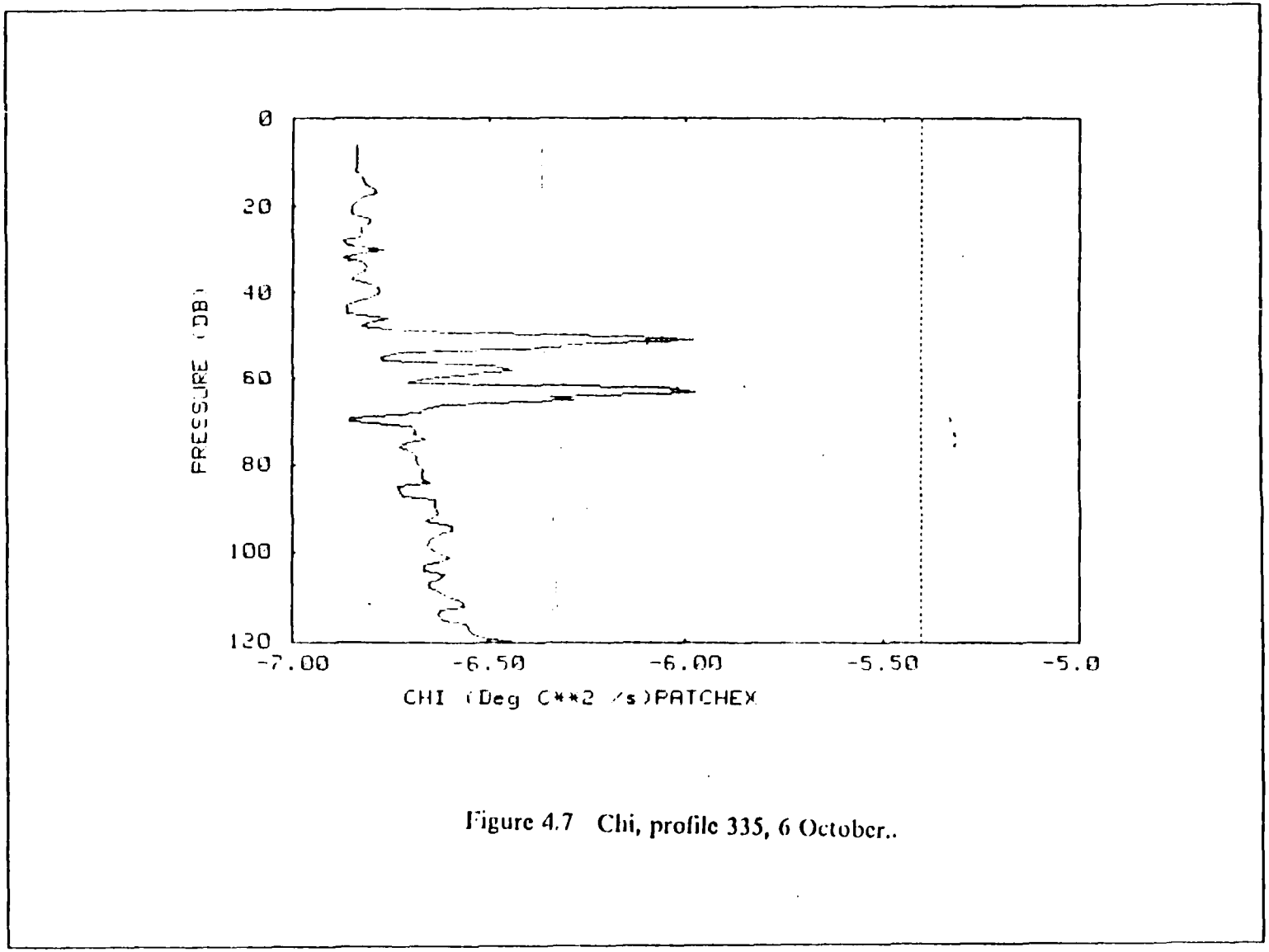

Figure 4.7 Chi, profile 335, 6 October..

B. HORIZONTAL VARIABILITY

Figure 4.8 illustrates two of the more salient features of the time series of temperature at 10, 20, 40 and 100 meters depth from 6-12 October. Most evident, is that the upper mixed layer warmed from 6-8 October when incomplete daytime mixing of the seasonal mixed layer was observed. During the remainder of the period, the upper ocean experienced virtually uninterrupted cooling with well mixed conditions prevailing throughout the mixed layer. These heating and cooling trends, which must be clearly reflected in an analysis of the total heat content, are examined in the next section. Barring significant horizontal advection or vertical temperature redistribution into the mixed layer from the thermocline below, the trends must reflect the surface forcing outlined in the previous chapter.

Also apparent in the time series of Figure 4.8 are the horizontal temperature trends which exist within the domain and evolve from pattern to pattern. They are difficult to quantify by inspection due to the irregular spacing which exists between similar measurements at a given depth. That is why the vertical lines which divide the time series into individual patterns are not equally spaced. The x-axis is the profile number and not distance or time. The variability of the ship speed and the towyo winch profile range is responsible for the difficulty in quantifying the trends. The character of these gradients or trends is more variable as depth increases below 20 meters. Inspection of Figure 4.8 clearly shows that there is vertical coherence of the time series at 10 and 20 meters depth. As one moves below the active surface mixing layer this coherence decreases. The structure of the time series is also clearly different. It is important to note that the range of the temperature variability along each leg at 40 meters is less for the first three patterns of the survey than is observed in the 10 meter time series for the same patterns. Care must be exercised when comparing the time series since each graph is scaled between the maximum and minimum temperature along the track covered and the ranges differ considerably both in depth and in time. Below the base of the mixed layer the presence of internal wave activity prevents the simple extraction of horizontal gradients. Correlation of the temperature and salinity time series at 10, 20 and 40 meters meters can be seen by comparing Figures 4.8 and 4.9.

To understand the temperature trends which Figure 4.8 depicts, time series from individual butterfly shaped patterns were plotted with the start and end of each leg of the sampling pattern marked. Figure 4.10 depicts similar time series for the first

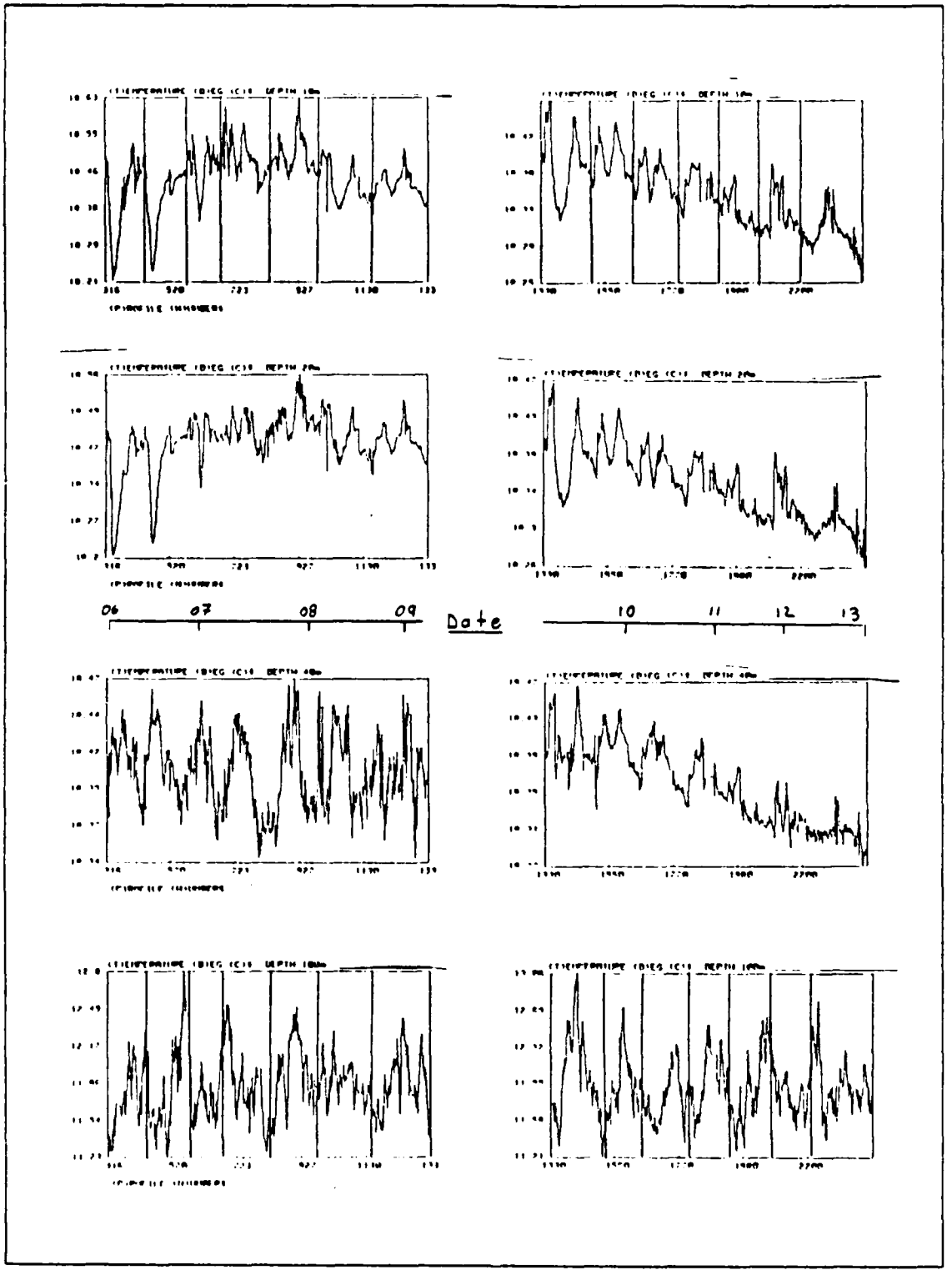

Figure 4.8 10, 20, 40 and 100 meter Temperature, 6-12 October.

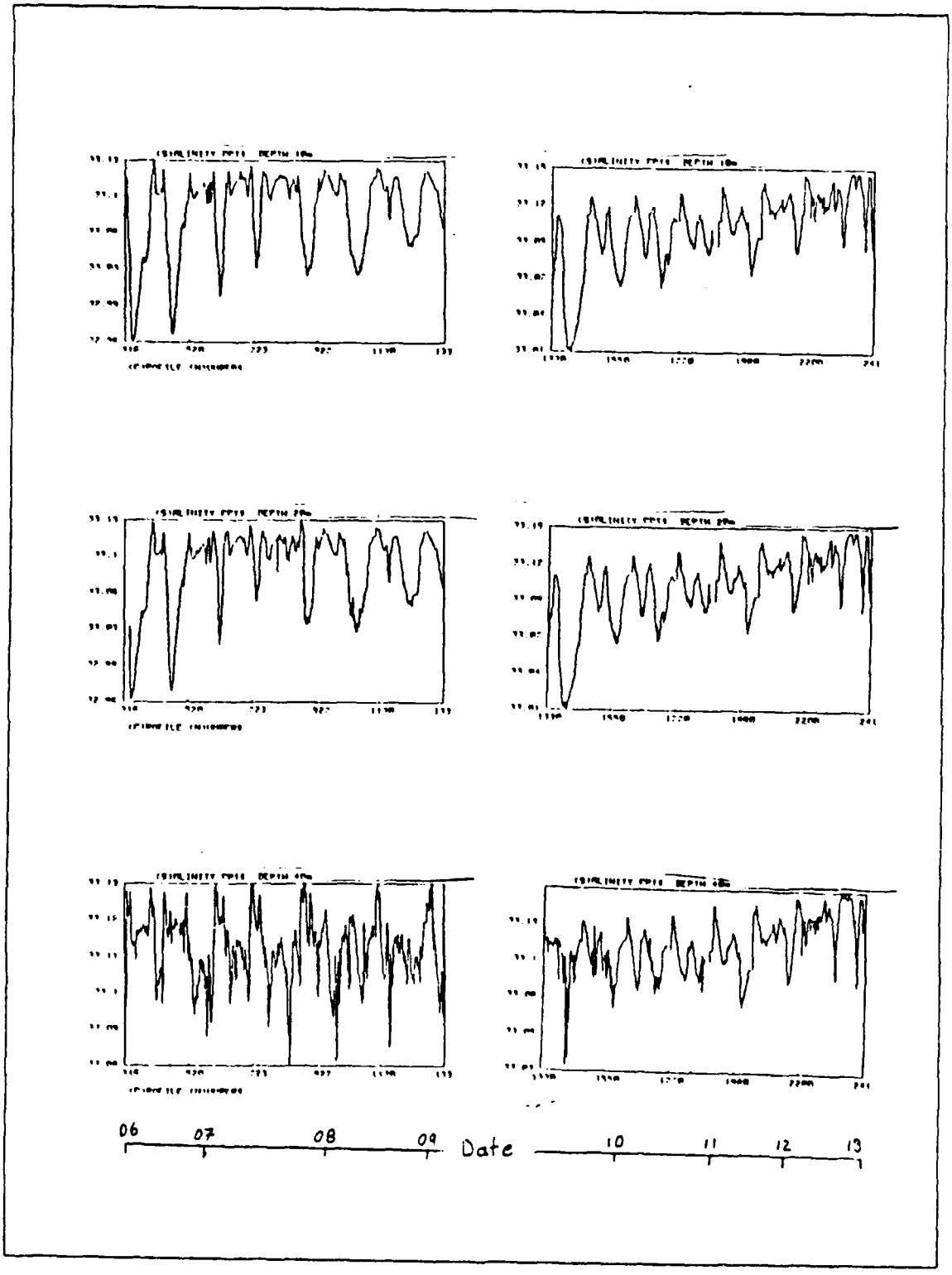

Figure 4.9 10, 20, and 40 meter Salinity, 6-12 October.

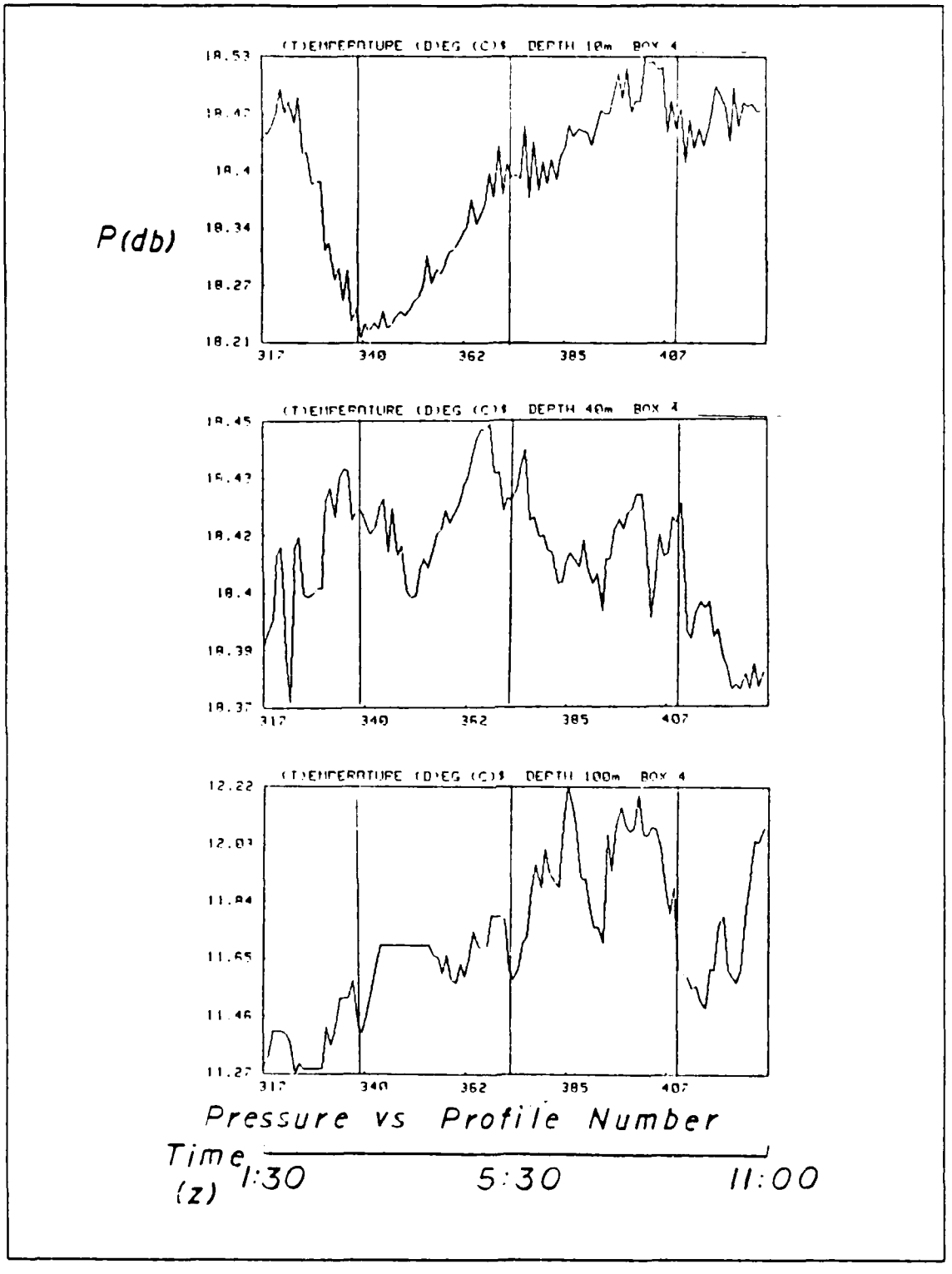

Figure 4.10 10, 40 and 100 meter Temperature, pattern 4.

complete butterfly pattern of the survey. The three vertical lines within the each of the graphs divide the patterns into their four component legs. The figure further illustrates the degree of spatial variability which exists within the domain and emphasizes that the earlier gradients appear stronger at 10 meters than at 40 meters. It also demonstrates in greater detail that the horizontal structure in the upper thermocline is dominated by internal wave activity and that mean horizontal gradients which may exist there can't be determined in this format.

Table 6 illustrates the magnitude of the temperature trends and the standard deviations of those trends from the starting to the ending profile number along the first leg (northwesterly) of each pattern at depths of 10, 40 and 100 meters. The standard deviations tabulated with each trend represent the square root of the residual variance

TABLE 6

TEMPERATURE TREND (MILLIDEGREES LEG) , LEG 1

Pattern	10 Meters	40 Meters	100 Meters
4	-253 ± 38	46 ± 12	-8 ± 145
5	-218 ± 32	83 ± 10	-725 ± 166
6	-46 ± 33	38 ± 10	-433 ± 252
7	2 ± 38	51 ± 10	-933 ± 130
8	66 ± 17	68 ± 14	623 ± 164
9	12 ± 26	-1 ± 24	-15 ± 192
10	95 ± 12	-40 ± 23	258 ± 129
11	11 ± 31	-3 ± 31	399 ± 190
12	57 ± 11	44 ± 16	95 ± 125
13	63 ± 9	61 ± 10	-302 ± 90
14	43 ± 12	40 ± 11	-301 ± 112
15	7 ± 8	4 ± 6	-211 ± 109
16	4 ± 5	-4 ± 5	-985 ± 143

of the leg after the trend is removed. In patterns 4-6 a significant negative temperature gradient apparently exists at 10 meters. Since the upper ocean was diluted by rainfall in the first several days of the experiment, these gradients are very likely due to the advection of warmer, dilute water from the northwest in connection with the prevailing north to northwesterly wind induced flow. Gradients, such as those observed, could be attributed to transitory synoptic mesoscale fronts, eddies or filaments if a sub-surface gradient were also observed. Since the active mixing layer does not extend below 35 meters (in some cases, and generally less in others) the gradient is probably not the result of mesoscale interactions. It is most likely connected with differential surface

heating and the advection of dilute surface water from a region of greater precipitation to the northwest. The variability in solar heating which was observed due to clouds could account for a portion of horizontal gradients but the principal contributor appears to be precipitation. The time series of salinity at 10 meters in Figure 4.9 begins with salinity increasing which corresponds to the northwest to southeast leg of pattern 4.

Dissimilar temperature trends develop at 10 meters in Table 6 after the period of precipitation. These gradients are more similar to their counterparts at 40 meters and in several cases are comparable. This occured when the convective mixing spanned the entire fossil mixed layer from 8-12 October. The higher variability which exists at 100 meters due to internal wave activity in the upper thermocline is illustrated in column 3 of Table 6. At 10 and 40 meters internal waves exhibit a minimum of visible influence on the thermal structure due to the lack of stratification in the mixed layer.

The temperature trends at 10 meters along the complete sections of each leg containing profiles from near the surface to 120 meters are summarized in Table 7.

TABLE 7

TEMPERATURE TREND (MILLIDEGREES LEG), 10 METERS

Pattern	Leg 1	Leg 2	Leg3	Leg 4
4	-253 ± 38	172 ± 18	31 ± 23	39 ± 20
5	-218 ± 32	164 ± 15	59 ± -7	16 ± 4
6	-46 ± 33	55 ± 14	84 ± 14	48 ± 23
7	2 ± 38	19 ± 28	-9 ± 14	5 ± 9
8	66 ± 17	-2 ± 19	14 ± 32	-29 ± 15
9	12 ± 26	-6 ± 19	79 ± 9	-7 ± 9
10	95 ± 12	25 ± 13	-3 ± 21	-53 ± 6
11	11 ± 31	32 ± 16	54 ± 9	-11 ± 3
12	57 ± 11	-48 ± 12	22 ± 9	-9 ± 6
13	63 ± 9	33 ± 14	-12 ± 2	
14	43 ± 12	-7 ± 2		-33 ± 8
15	7 ± 8	-22 ± 16	-16 ± 4	-18 ± 6
16	4 ± 5	3 ± 15	24 ± 4	0 ± 5

Complete timeseries exist along legs 1,2 and 4 while only the first half of leg 3 was utilizable. The second half of leg three was interrupted with deep tows and tows at constant depth and was necessarily omitted. To appreciate the extent of the gradients involved, the lengths of the survey legs described above average 11.2, 8.0, 5.6 and 8.0 kilometers for legs 1-4 respectively. Patterns 4-6 of Table 7 depict the stronger

temperature trends which existed along all four legs during the pre-convective period for the mixed layer. In subsequent patterns the large standard deviations indicate that significant local temperature gradients often overshadow the smaller trends.

Table 8 summarizes the time series of temperatures at 40 meters.. The stronger trends observed in the first three patterns of Table 7 at 10 meters are smaller in Table

TABLE 8

TEMPERATURE TREND (MILLIDEGREES/LEG) , 40 METERS

Pattern	Leg 1	Leg 2	Leg3	Leg 4
4	46 ± 12	25 ± 11	-30 ± 6	-41 ± 8
5	83 ± 10	-146 ± 8	18 ± 6	1 ± 9
6	38 ± 10	-32 ± 13	63 ± 16	20 ± 11
7	51 ± 10	-11 ± 6	-2 ± 6	9 ± 7
8	68 ± 14	21 ± 56	-75 ± 18	37 ± 16
9	-1 ± 24	-17 ± 12	-50 ± 18	18 ± 10
10	-40 ± 23	-3 ± 9	-2 ± 21	16 ± 8
11	-3 ± 31	-14 ± 11	37 ± 16	-4 ± 4
12	44 ± 16	-33 ± 8	1 ± 11	-14 ± 3
13	61 ± 10	-18 ± 10	-8 ± 2	-14 ± 4
14	40 ± 11	11 ± 6		-33 ± 6
15	4 ± 6	-22 ± 16	-18 ± 5	-12 ± 6
16	-4 ± 5	-13 ± 15	19 ± 8	3 ± 5

8. Although convective conditions extend throughout the entire mixed layer after patterns 4-6, the trends at 40 meters do not accurately reflect those at 10 meters for several days. Near the strongest convection period toward the end of the study, the fossil mixed layer is nearly homogeneous and there is almost a 1:1 correspondence in trends at 10 and 40 meters. This can be seen by comparing the trends in Tables 7 and 8 for patterns 15 and 16 where there is very little horizontal structure.

C. MIXED LAYER HEAT CONTENT

In the previous chapter on surface fluxes, Figure 3.7 showed two distinct periods. From 06 to 08 October, a diurnal cycle occurred in which Q_0 alternated between +5 MJ m^2 during the day and -5 MJ m^2 at night. Over the next four days, 8-12 October, there was a net loss of heat at the ocean's surface of 35 MJ m^2. This cooling can also be seen in Figure 4.11, the time series of total heat in the mixed layer.

Equation 1.2 was integrated to the base of the mixed layer to produce the time series in Figure 4.11. To ensure that colder temperatures below the base of the mixed layer were not included in the integration, the average temperature of the layer was

integrated to an arbitrary depth (1 meter) above the top of the thermocline. This method accounts for approximately 2 percent heat content loss over an average depth of 50 meters in a completely isothermal mixed layer. The discrepancy is preferable to the cold water contamination that that would occurr across the base of the mixed layer due to internal waves if the integration were performed all the way to the mixed layer depth.

Based on a 14 percent maximum error in cumulative net heating, the cumulative Q_0 at the ocean surface was 35 ± 5 MJ/m^2. Integrated over the average depth of the mixed layer (50 meters) the surface flux represents a loss of 0.7 ± 0.1 MJ m^3 of total heat content. Figure 4.11 shows that during the same period the loss of total heat in the mixed layer is approximately 0.6 to 0.8 MJ m^3. This is consistent with the latent and sensible heat loss being the primary heat transfer mechanisms during the period. The moderate wind conditions during PATCHEX were clearly sufficient enough to remove a significant amount of heat from the ocean surface and to mix the warm, semi-stratified, daytime surface layer into the entire mixed layer.

It is important to consider how much of the wind stess translated into vertical entrainment of colder water below the base of the mixed layer. Large *et. al.* (1986) determined that strong storms accounted for most of the autumnal cooling of the sea surface. During a storm event, one would expect vertical entrainment to be a primary factor in the overall heat content of the mixed layer. The period of this study was one of moderate winds where low relative humidity coupled with decreased insolation allowed substantial cooling of the ocean surface without significant erosion of the mixed layer (or entrainment of cooler water). Given the errors in the fluxes, however, it is important not to discount the possibility of vertical entrainment at the base of the mixed layer. Vertical entrainment might account for the observed error in the balance or it may be offset by horizontal advection. Barring the presence of mesoscale currents to provide net transport, horizontal advection is a questionable cooling mechanism for this period. In summary, since there were no storm episodes during PATCHEX, it is understandable that the heat content balances well with the large surface fluxes.

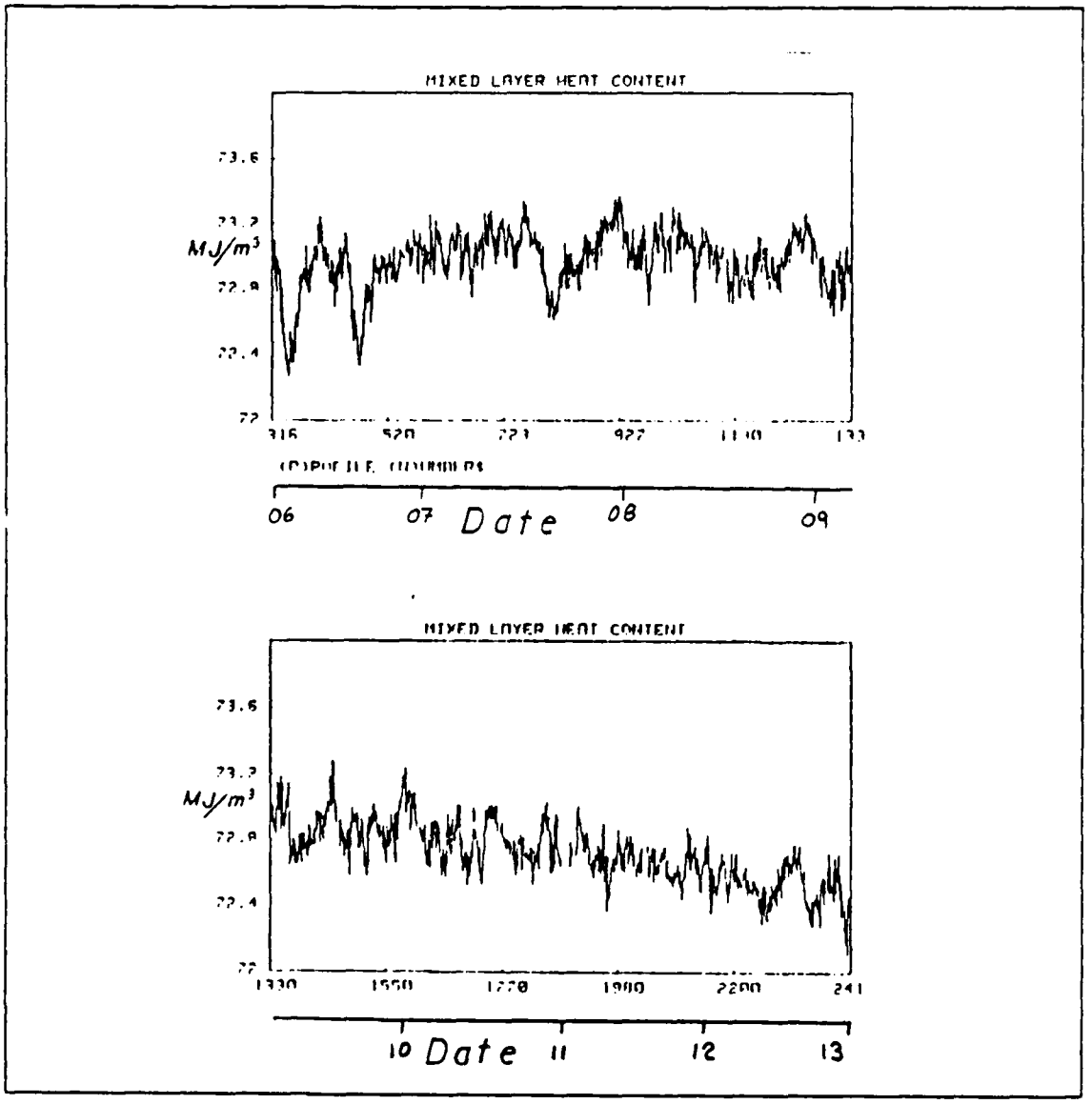

Figure 4.11 Mixed layer heat content, 6-12 October.

V. HORIZONTAL GRADIENTS BY OBJECTIVE ANALYSIS

A. THEORY AND TESTING OF THE O-A

The space-time series of temperature at constant depth were mapped on to a uniform grid using an objective analysis routine written by J. Smith at the Naval Postgraduate School and recently adapted for PATCHEX. This analysis was undertaken in order to develop quasi-synoptic snapshots for each of the 13 consecutive survey patterns this thesis employs. The algorithm is based on the work of Bretherton et al (1976) which used MODE (Mid Ocean Dynamics Experiment) data to develop a successful oceanographic application of interpolator/extrapolator techniques which had been developed earlier for meteorological analyses (Gandin, 1965). The program employs a simple 3 dimensional radial search in X and Y space and in time to find seven scalar values closest to each gridpoint. Values are taken from each profile at a given depth, γ_x, equal to the magnitude of the scalar of interest (temperature in this case) and added to an estimate of the random noise associated with the measurement, *i.e.*

$$\gamma_r = \theta_r + \varepsilon_r. \qquad (\&5.1)$$

The objective analysis then uses those values to estimate the value of the scalar and its error at successive grid points within the PATCHEX domain. To produce this spatial depiction, the algorithm uses pre-determined correlation scales to map the scalar onto a uniform grid.

Determining the correlation length for the data in each pattern was complicated by the irregular spacing and sampling interval between successive measurements of scalar quantities at a given depth. To determine the autocorrelation length of the data, an autocorelation function was generated by calculating a radial lag between successive data points along the survey track and every other point in the data field. The autocorrelation was then calculated using the standard formula

$$R_r = (\gamma_r - \gamma)(\gamma_{r+\delta r} - \gamma)/\sigma^2 \qquad (5.2)$$

where r is the radial lag. This method assumes an isotropic data field.

A graphic depiction of the radial correlation function was produced by dividing a 8 kilometer radius into 20 bins and accumulating autocorrelation values into respective bins every 0.4 kilometers from the origin. Figure 5.1 depicts the correlation function for a typical survey pattern. The modal value of the correlation radius for the 13

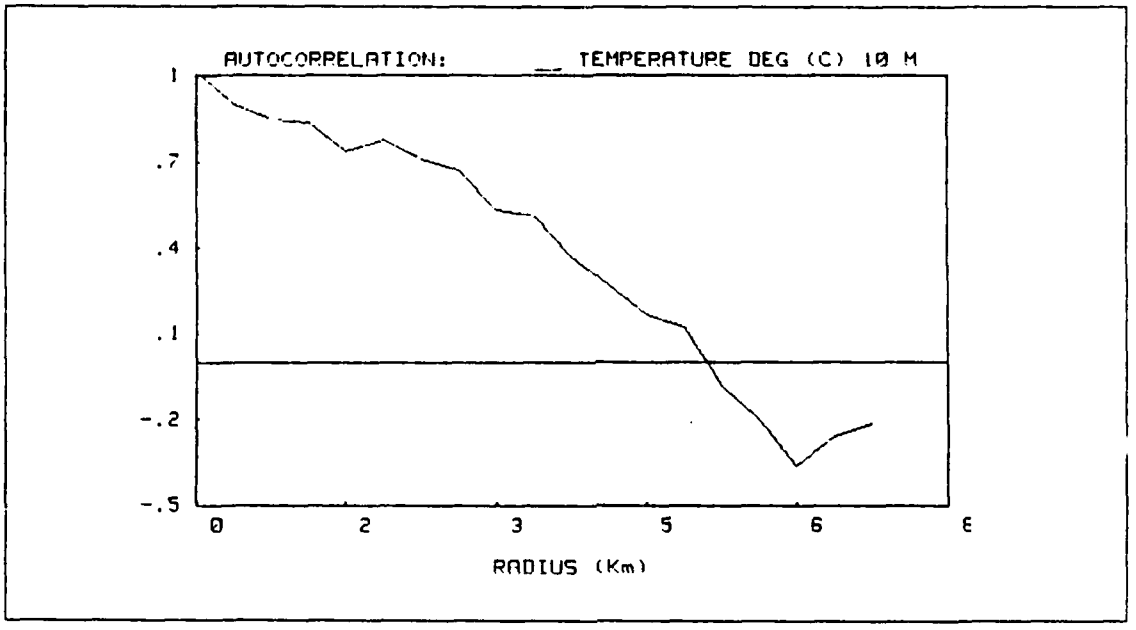

Figure 5.1 Typical correlation function, pattern #4.

patterns that this study employs is approximately 6 kilometers. Since the data set is finite in size and the algorithm divides the abcissa of 8 kilometers into 20 bins, the method does not perfectly reproduce the shape of a continuous autocorrelation curve. It does, however, effectively determine the radius at which the data becomes decorrelated.

A default correlation length, R_0, of 12 kilometers was applied in the objective analysis. The correlation function it uses is double sided and our correlation radius as determined earlier is 6 kilometers. Specifically, the correlation function used in the objective analysis is

$$F = (1-R_f)\, e^{(-R_f/2)} \qquad (5.3)$$

where the three dimensional correlation scale, R_f is defined as

$$R_f = (X^2 + Y^2)\, R_0^{\,2} + T^2 / T_0^{\,2}. \qquad (5.4)$$

Note that the correlation function includes a time scale. In this analysis, it was defeated, assuming that each pattern was sampled synoptically. The average elapsed time of each survey pattern ranged between 6-11 hours. 8 hours was roughly the average. Earlier patterns were surveyed more slowly than later ones.

After the data were run through a convolution filter, the default correlation scale of 12 kilometers was applied along with an error coefficient, $\varepsilon_r = 0.2$. This value of ε_r represents the average percentage of noise along each leg of each pattern in the survey. Testing showed that the objective analysis is not particularly sensitive to $\varepsilon_r < 0.5$. The average of the high end of the observed noise (20 percent) proved adequate in reproducing the resolvable temperature trends in each pattern without over-smoothing.

Before the actual data could be mapped, however, additional testing was undertaken. The O-A routine was tested with 2 fields, a south to north temperature gradient and a temperature spike imbedded in the gradient. The spike proved useful in tuning the filtering and correlation coefficients for later application in the actual analysis. It was located in the southwest corner of an 18.0-18.4°C south to north temperature gradient. The $\nabla_h T$ of 0.4 degrees over 12 kilometers was a representative temperature gradient in the same range as the time series observed in PATCHEX. The spike consisted of four adjacent points having a value of 18.3°C. The overall size of the input grid was 12 by 12 kilometers and the data were 400 points spaced 0.6 kilometers apart. The input grid is contoured in Figure 5.2. It depicts a maximum closed temperature contour of 18.24°C surrounding the spike. The S-N temperature gradient is also apparent in the figure.

The first test of the objective analysis was made using a correlation length, R_0, of 2 kilometers to more easily resolve the 0.6 kilometer spaced data. Results of that O-A were then contoured on the same grid used for the input field and are depicted in Figure 5.3. The input array had been subjected to various filter and error coefficents as well as different correlation lengths. The output array was best resolved using atriangular convolution filter over ± 4 points, an error coefficient of 20 percent and a 2 kilometer correlation length. Using these input parameters, an 18.20 maximum closed contour was analyzed.This represents an an 8 percent error in the estimate of the spike test function by objective analysis. Although various combinations of the input parameters were tested to produce the final field, the figure represents the best mix of

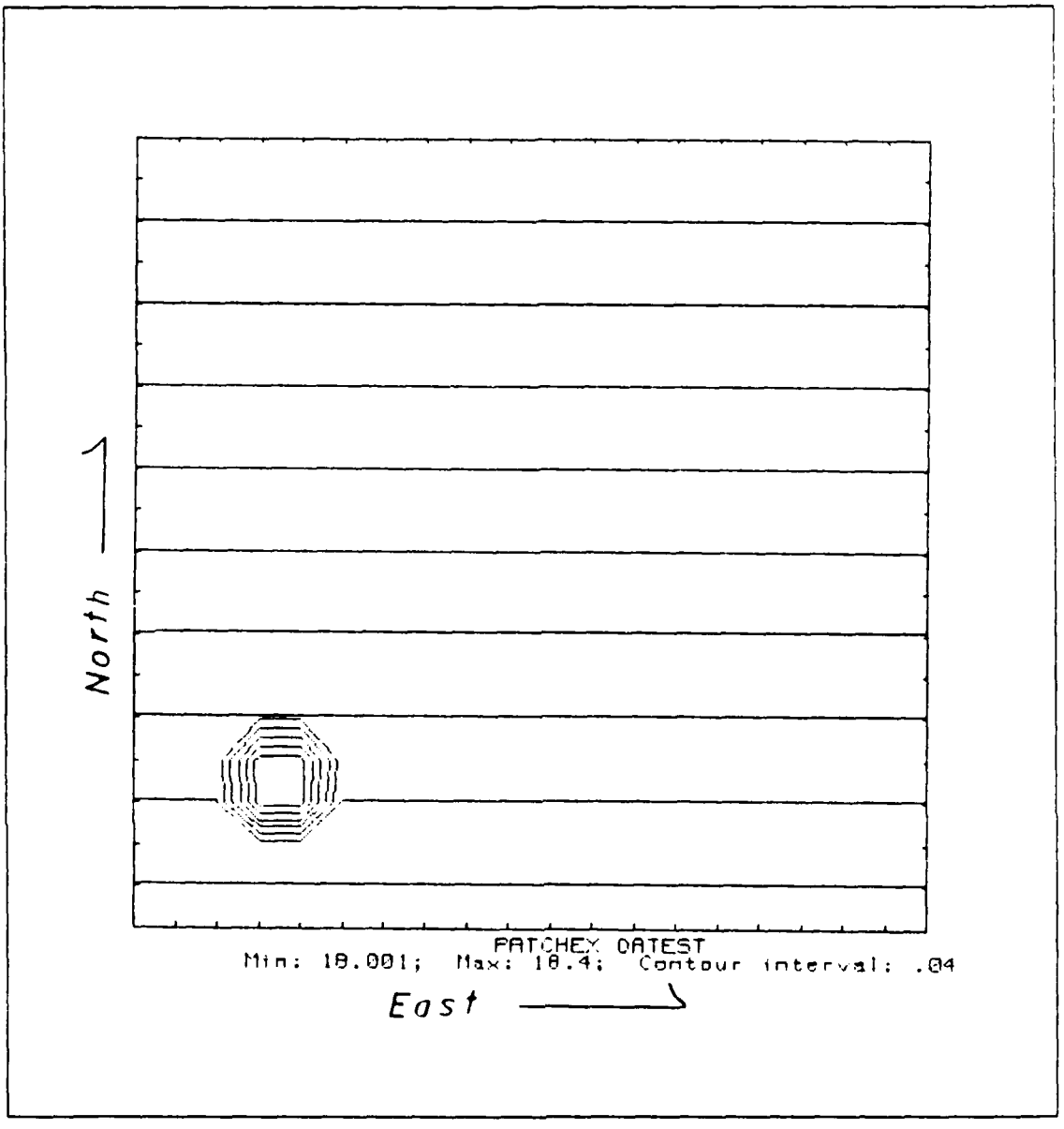

Figure 5.2 12 km N X 12 km E, O-Λ test input field.

those parameters which are still germane to PATCHEX. The convolution filter was used to reduce high frequency internal wave noise in the input field. The error coefficient was estimated from the high frequency content of each PATCHEX pattern used. The 2 kilometer correlation length tested the ability of the algorithm to better resolve localized features. Since the actual correlation length scale of the PATCHEX data is 12 kilometers, the data were re-tested using the higher value. This resulted in an

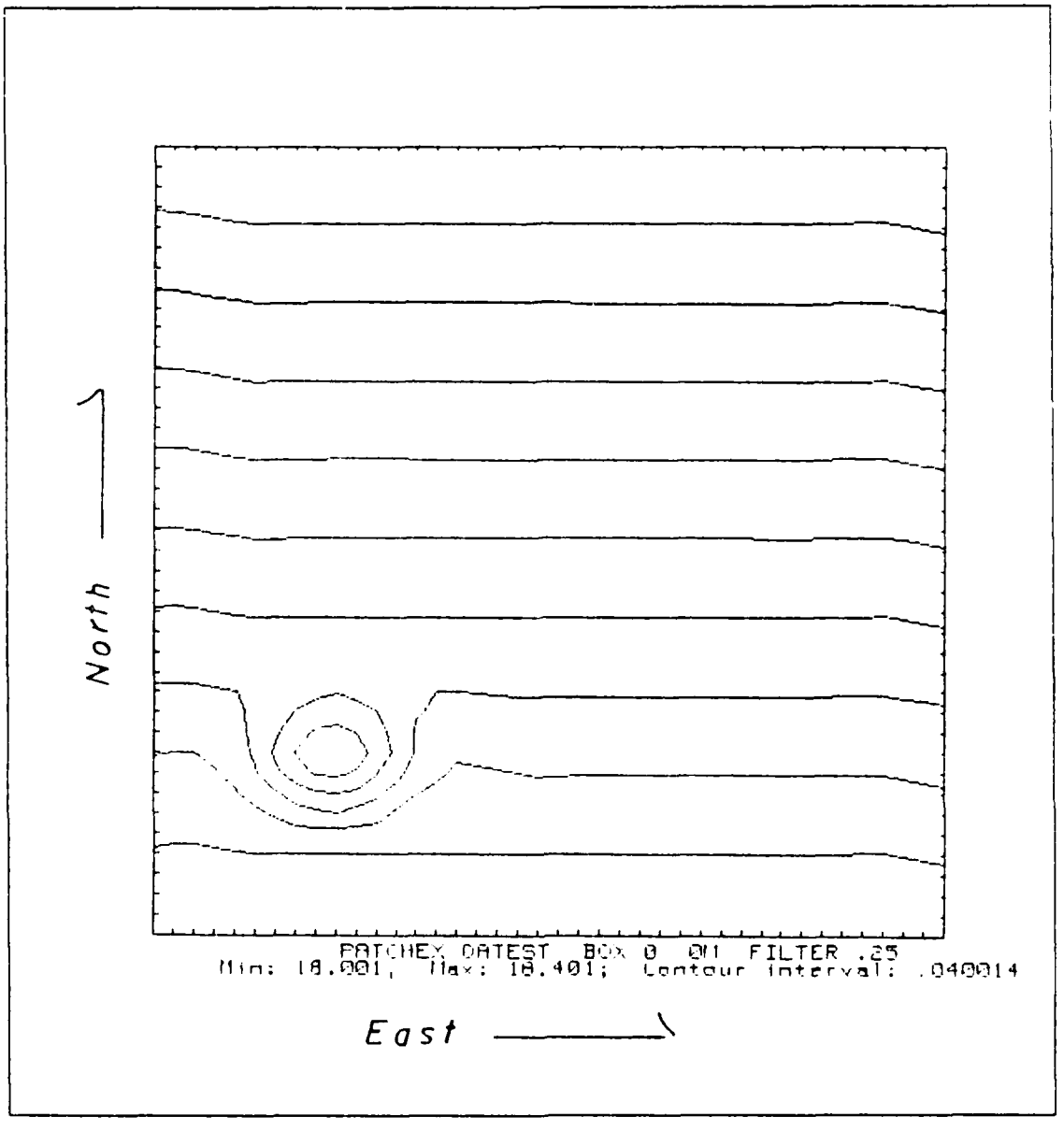

Figure 5.3 12 km N X 12 km E, O-A test output field, R_0 = 2 km.

expected loss of resolution of higher spatial frequency features. Since the actual scale of the test field was less than a kilometer, a 12 kilometer correlation scale is inappropriate for the high spatial frequency of the test data. The results of the analysis can be seen in Figure 5.4 where the largest resolved closed contour is 20.16°C. The artifact at the center of the contour indicates further error in the analysis. The next section will show that a larger R_0 is more applicable to the PATCHEX field, which is well correlated to 12 kilometers.

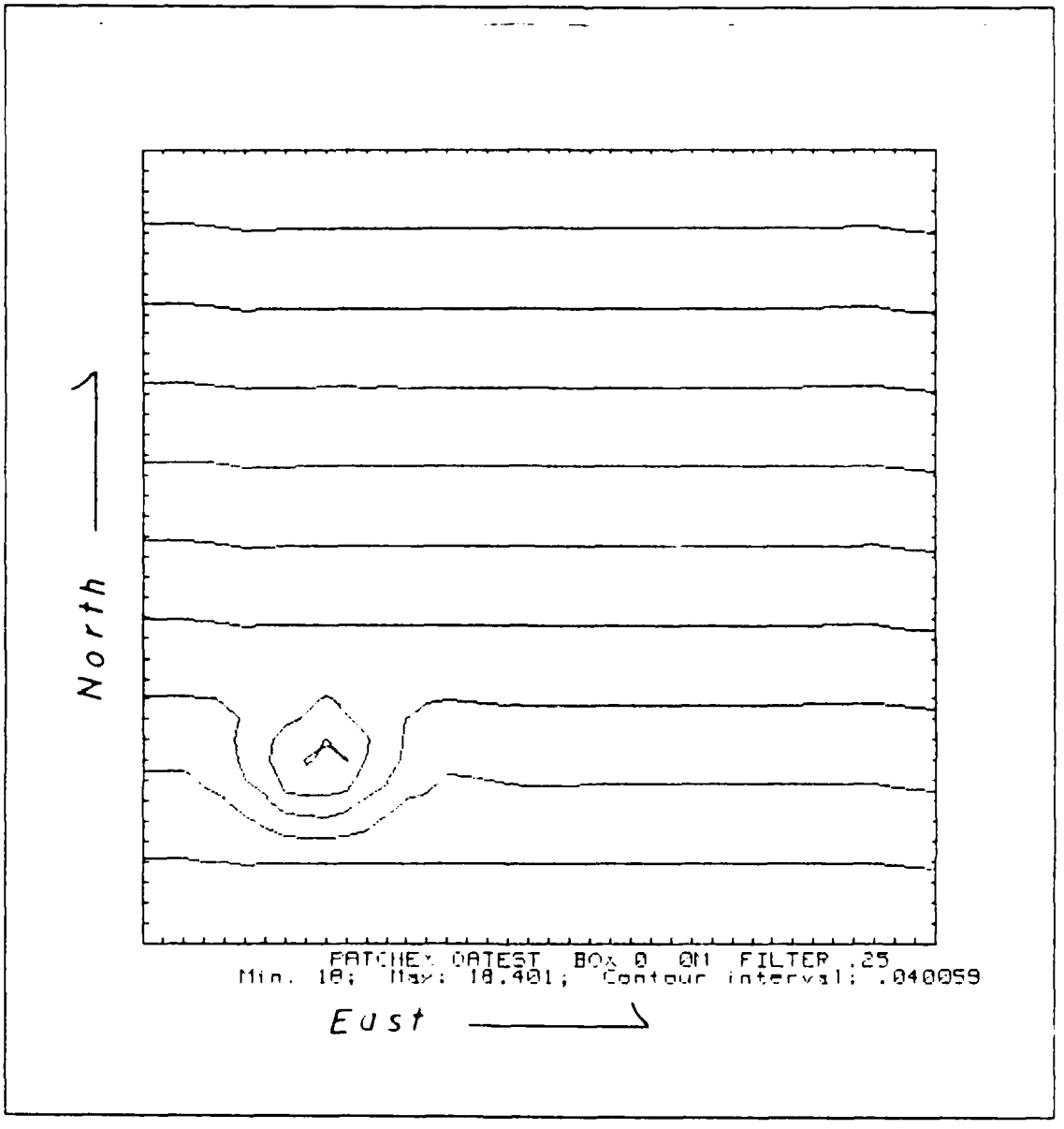

Figure 5.4 12 km N X 12 km E, O-A test output field, R_0 = 12 km.

B. RESULTS OF THE OBJECTIVE ANALYSIS OF PATCHEX DATA

The objective analysis was applied to the PATCHEX data using the input parameters described in the last section. The correlation scale was 12 kilometers. The results of the analysis are depicted in Figure 5.5. Also overlayed in the figure is the

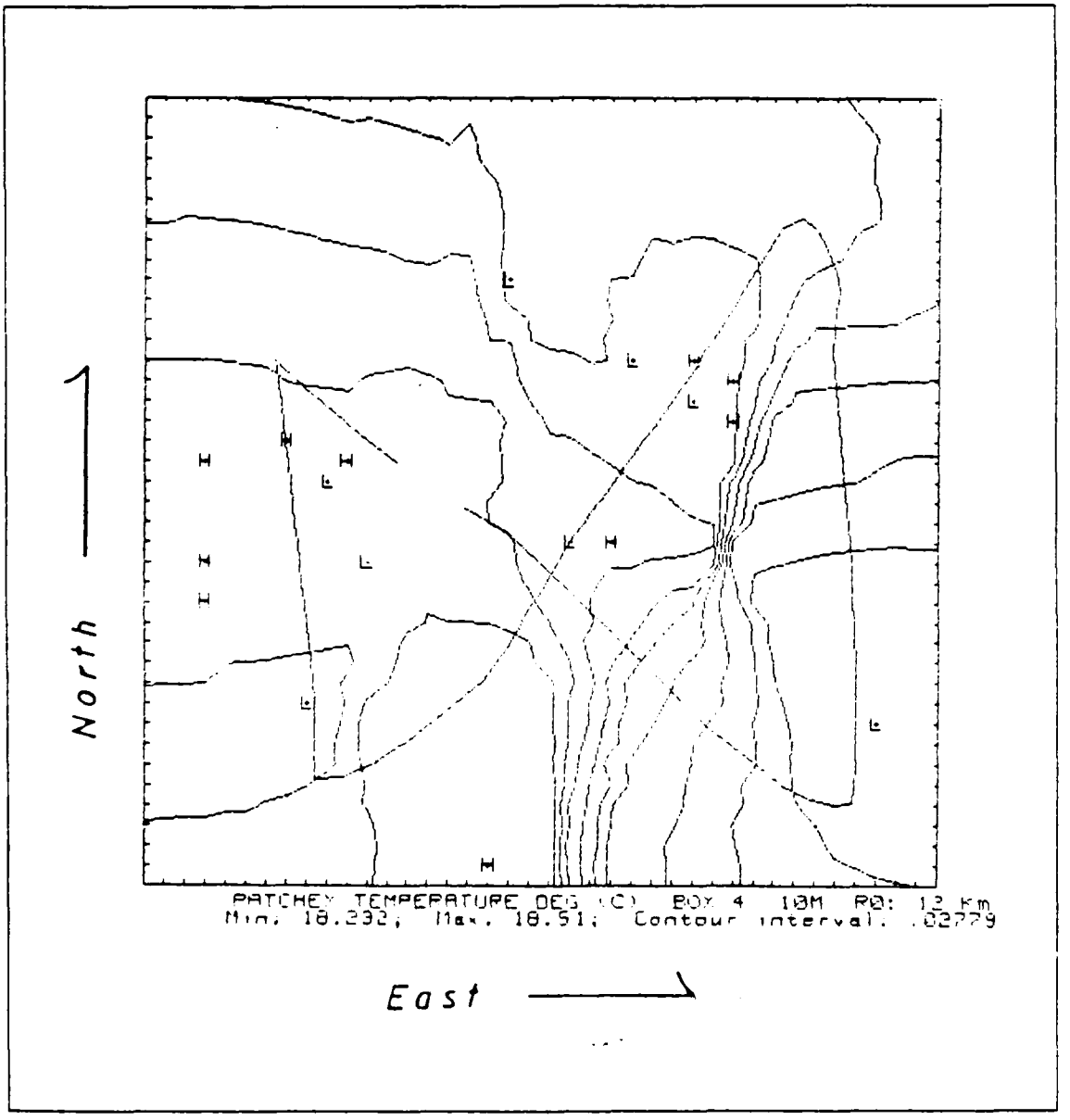

Figure 5.5 10 meter temperature, pattern 4, 14 km N X 14 km E, R_0 = 12 km.

butterfly shaped ship's track. The objective analysis was mapped on to a 14 X 14 kilometer grid of 1600 (40 X 40) points. The error field was also computed and is

depicted in Figure 5.6. It indicates that the objective analysis was able to produce accurate estimates of the temperature along the survey track but was only marginally successful in calculating the rest of the field. As would be expected, the regions outside the track and at the center of the two halves of the pattern exhibited especially high errors.

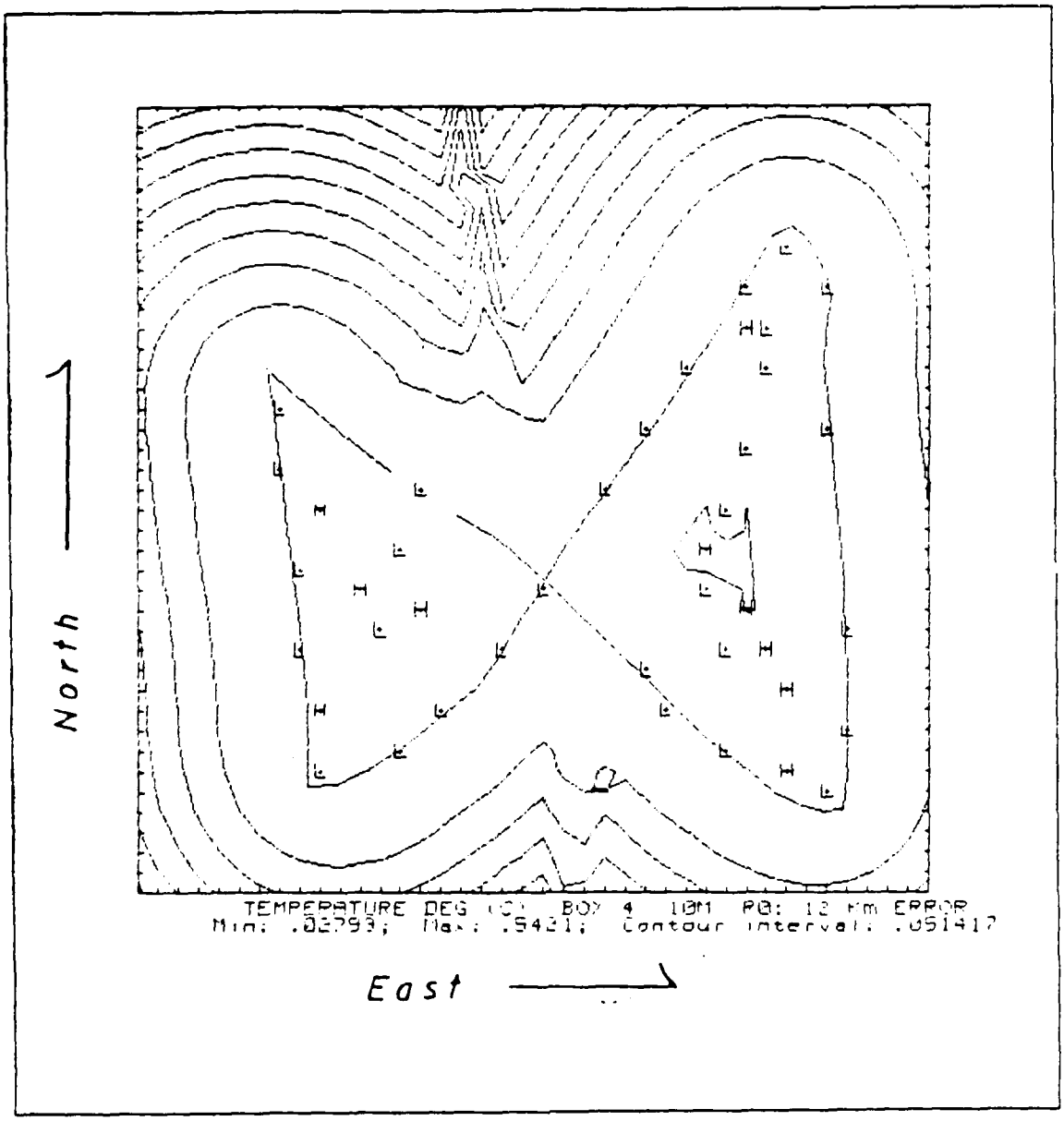

Figure 5.6 10 meter temperature error, pattern 4, 14 km N X 14 km E, R_0 = 12 km.

Inspection of the analysis in Figure 5.5 shows that the along-track temperature trends correlate extremely well with those in Table 6 of Chapter IV. It further shows that the general horizontal temperature gradient is decreasing from the northwest to the southeast which also appeared in Table 6. Warmer, more dilute surface water clearly exists in the northwestern regions of the domain as was suspected in the earlier description of the raw temperature time series. The most erroneous feature in the objective analysis is the extreme gradient located at the center of the eastern half of the survey pattern. This is substantiated in the error analysis of Figure 5.6.

Various attempts were made to adjust the input coefficients to better resolve the fields by objective analysis. Attempts were even made to decrease the correlation time scales and reduce the effect of temporally distant data. This approach was rejected after the incomplete fields provided extremely erroneous and noisy results. The effect of decreasing the correlation length in order to better resolve localized trends are seen in Figures 5.7 and 5.8. Using a 6 kilometer correlation length, Figure 5.7 was able to better isolate the trends along the survey track but increased the off-track noise. Also, the actual values of the along-track trends resulting from applying a decreased correlation length were no more accurate than those in Figure 5.5. Further reduction of the correlation length to 3 kilometers only exacerbated the error away from the track. This is depicted in Figure 5.8.

Having confined our choice of correlation length, filter coefficient and error criteria, it was decided to apply the OA only to depict the trends along those survey patterns whose trends were substantially greater than their associated noise values (variances) as tabulated in Tables 7 and 8. This decision proved correct as the OA had performed poorly in analyzing pattern 4 which contained the most significant temperature trends. Testing of subsequent patterns indicated that as the mixed layer became more homogeneous, with less defined large-scale gradients, the OA lost the ability to discriminate the trends. Since the first three patterns of the survey covered a period when a surface layer with significant horizontal gradients existed, those patterns contained trends greater than the order of the high frequency noise within the domain. Pattern 6 contained the last clearly resolvable horizontal trend at 10 meters. Following pattern 6, the trends are lost in the noise and the O-A begins to create artifacts. Despite the noisier subsequent patterns, Figures 5.9 and 5.10 depict the decreasing temperature trend from the northwest to the southwest corner as in Figure 5.5.

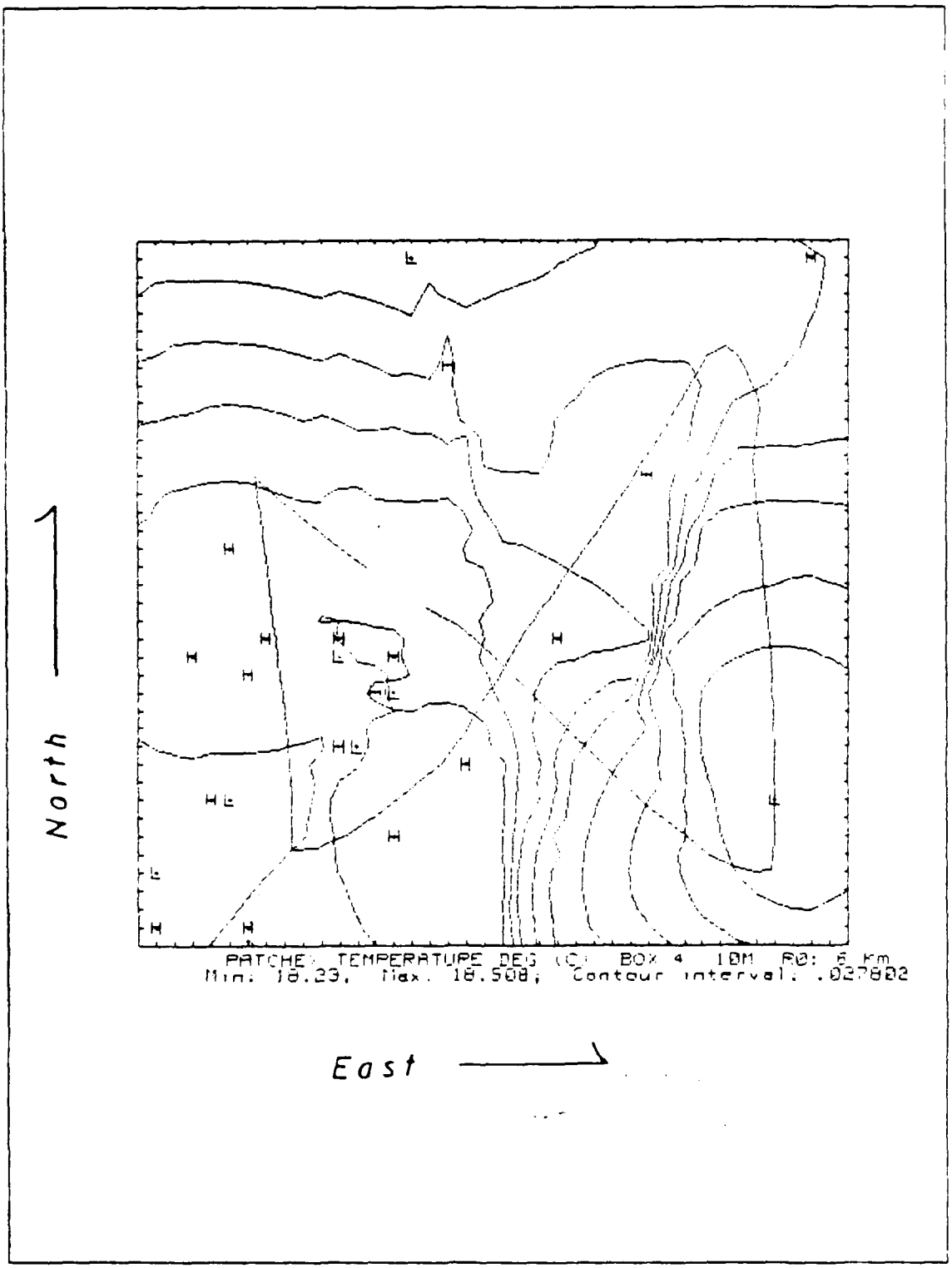

Figure 5.7 10 meter temperature, pattern 4, 14 km N X 14 km E, R_0 = 6 km.

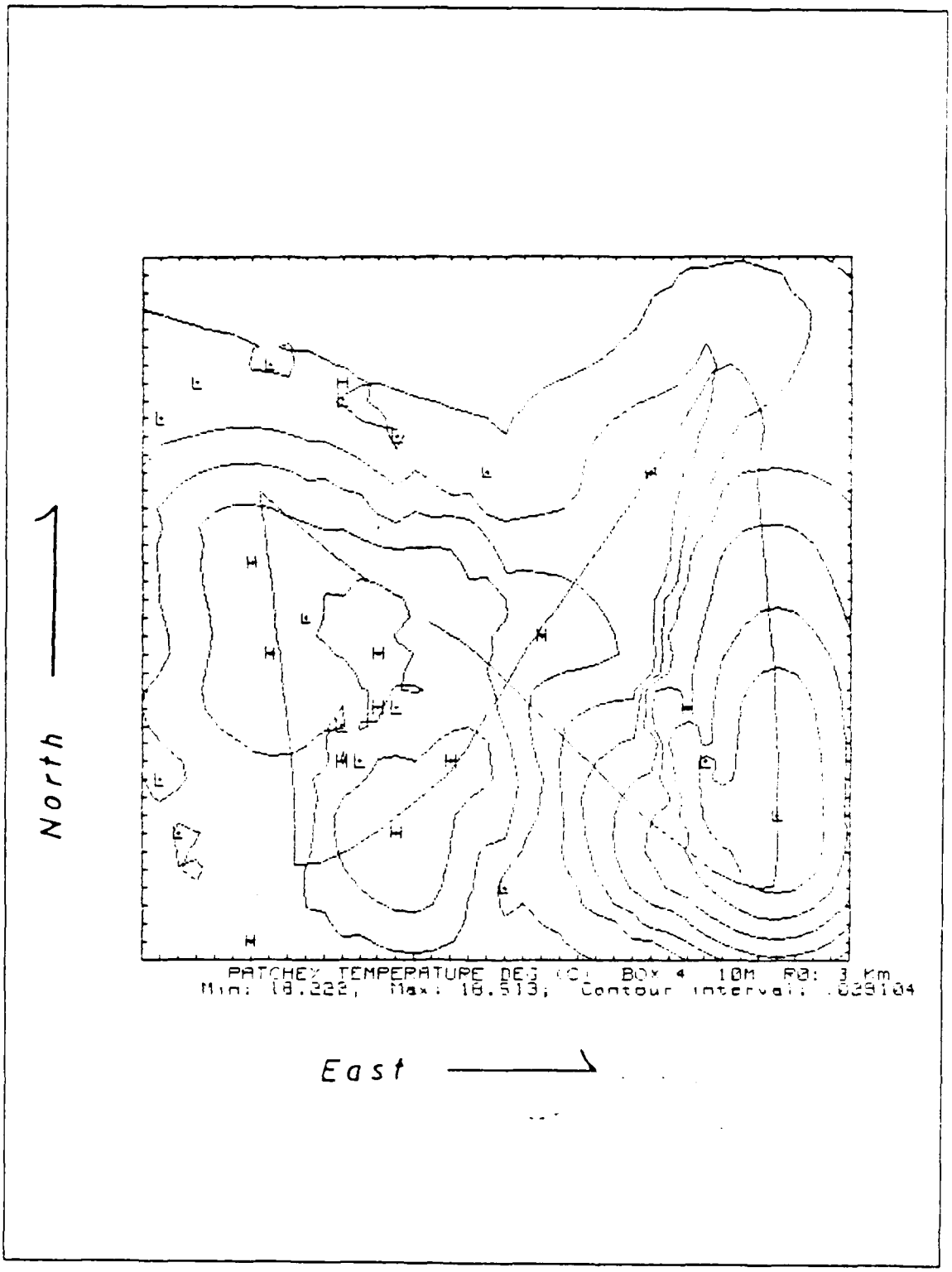

Figure 5.8 10 meter temperature, pattern 4, 14 km N X 14 km E, R_0 = 3 km.

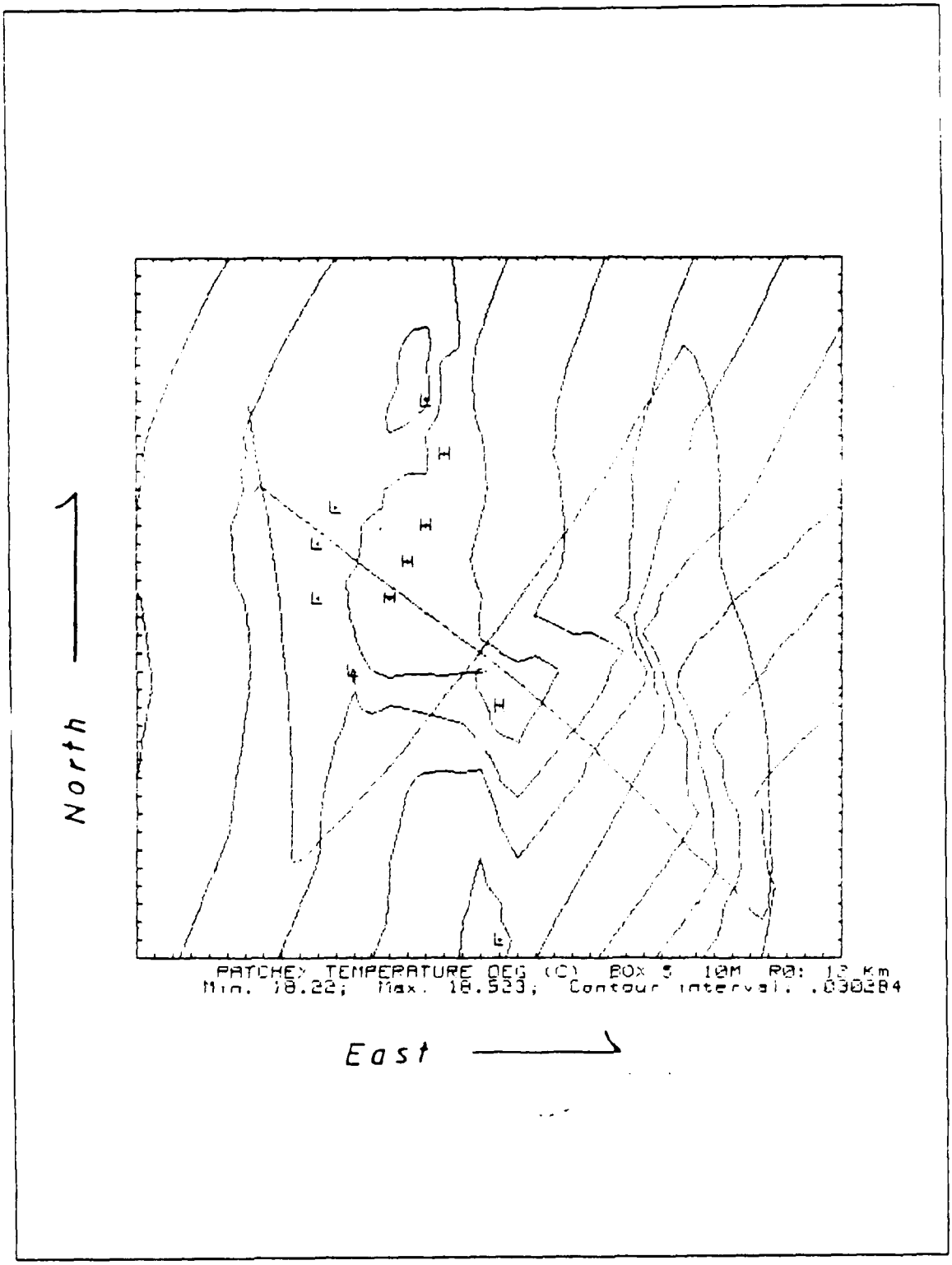

Figure 5.9 10 meter temperature, pattern 5, 14 km N X 14 km E, R_0 = 12 km.

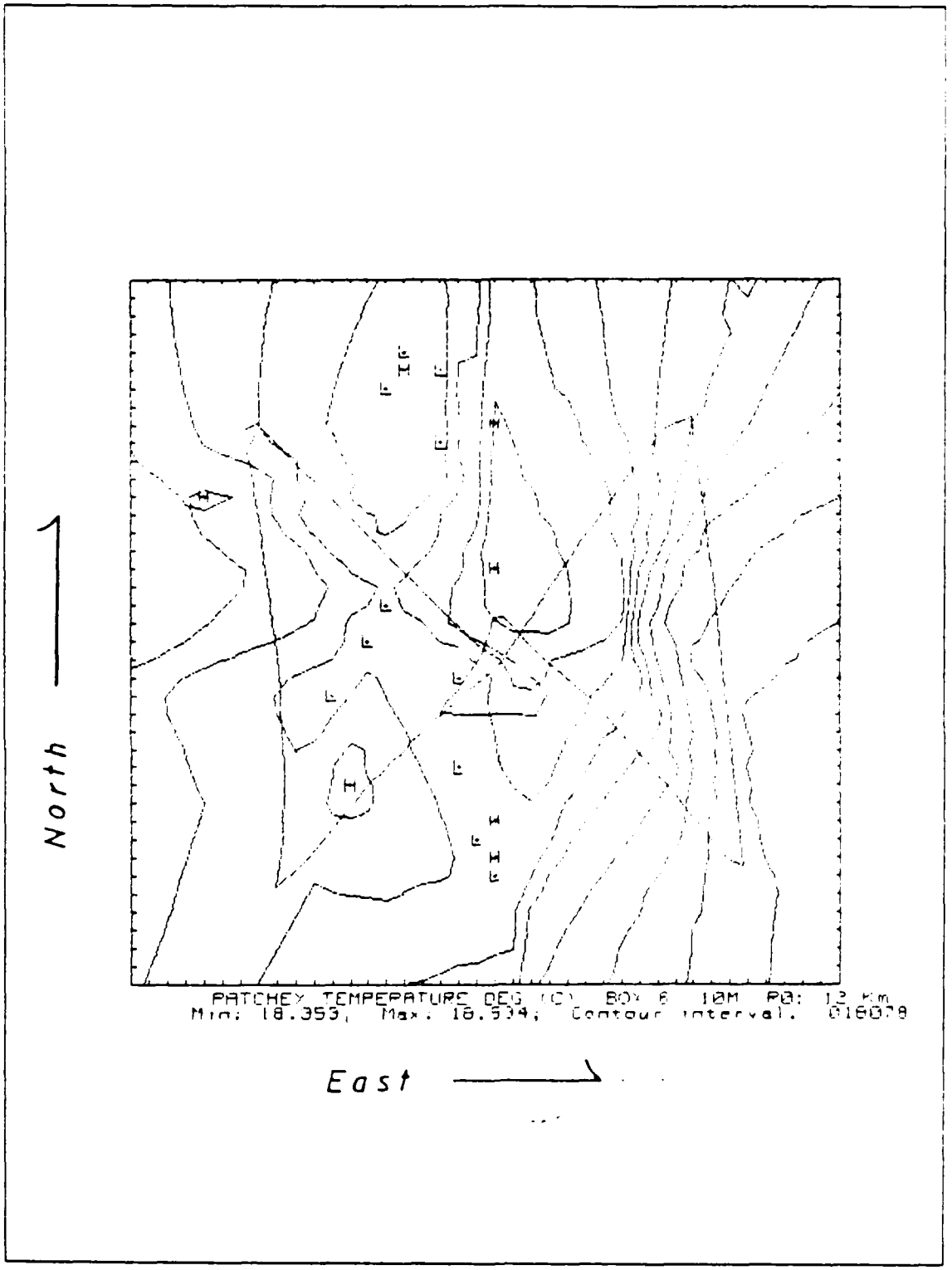

Figure 5.10 10 meter temperature, pattern 6, 14 km N X 14 km E, R_0 = 12 km.

Similar results were obtained using the data at 40 meters. Again, the first three patterns of the study provided the best results. As in the 10 meter analyses, the gradients along the track were mapped correctly but the rest of the domain suffered very high errors. The results of the analyses at 40 meters for the first three patterns can be seen in Figures 5.11 through 5.13. Note that these analyses resolved the overall trends at 40 meters more clearly in Figures 5.12 and 5.13 than in Figure 5.11. Since this region is below the actively mixing surface layer and near the base of the fossil mixed layer, communication with the upper thermocline may temporally alter the temperature field. Internal waves, convective compensation processes near an intrusion and vertical transport over the 8 hour survey cycle can all contribute to quickly change the horizontal temperature distribution near the base of the mixed layer. Despite these variations, which are extremely small in magnitude and not easily resolved, the O-A was still able to portray the general horizontal distribution of temperature at 40 meters in the first 3 patterns.

Inspection indicates that there is a positive west to east temperature gradient in each of these patterns. This further implies that the surface layer and the fossil mixed layer are completely decoupled during the first two days of the study. The temperatures at 40 meters are also cooler than the temperatures at 10 meters during the two day period when convective mixing of the fossil mixed layer and the surface layer was curtailed. These results support the hypothesis that a warmer, saltier, northwesterly moving layer of surface water inhabits the PATCHEX domain on 6-8 October 1986.

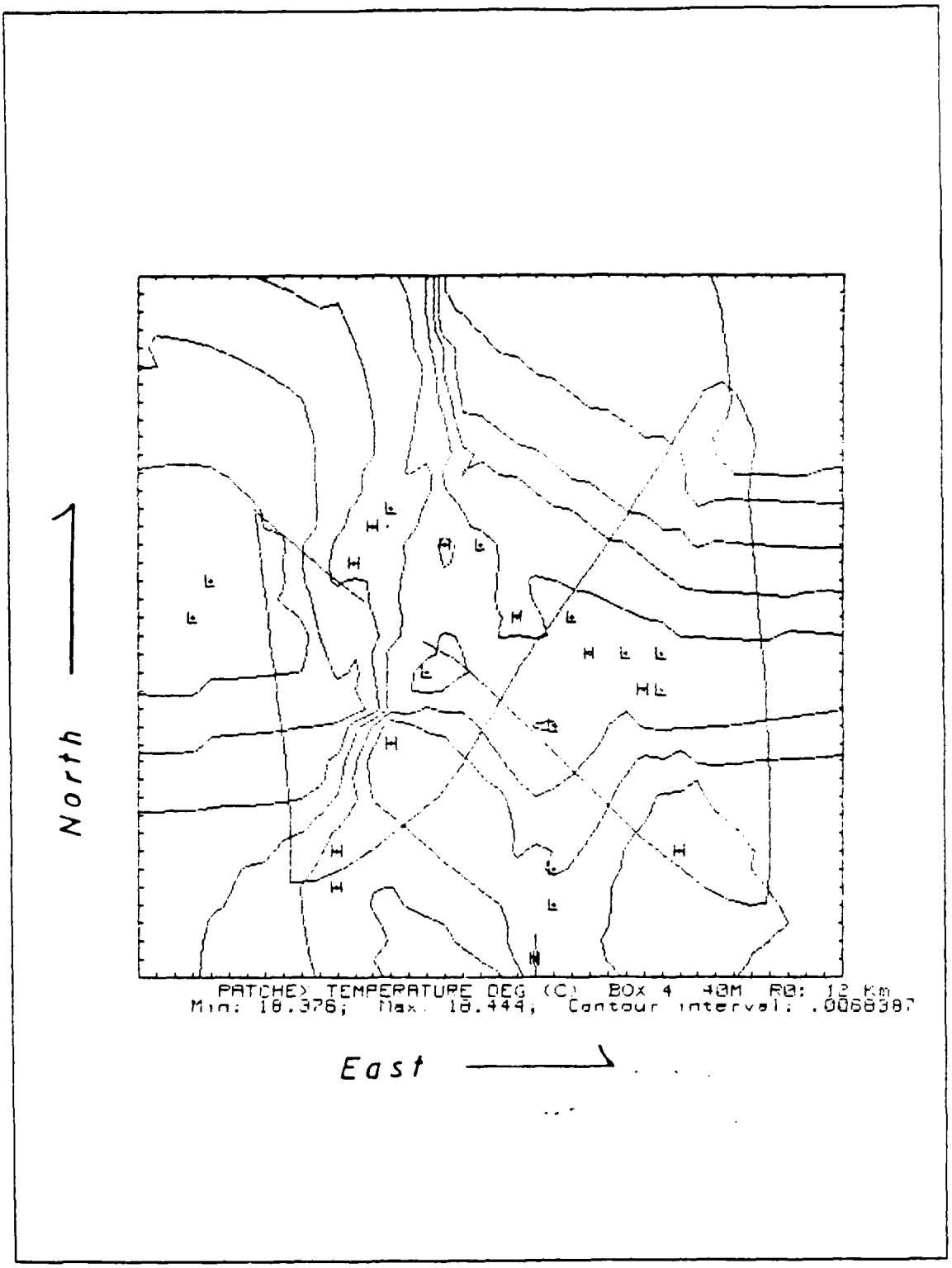

Figure 5.11 40 meter temperature, pattern 4, 14 km N X 14 km E, R_0 = 12 km.

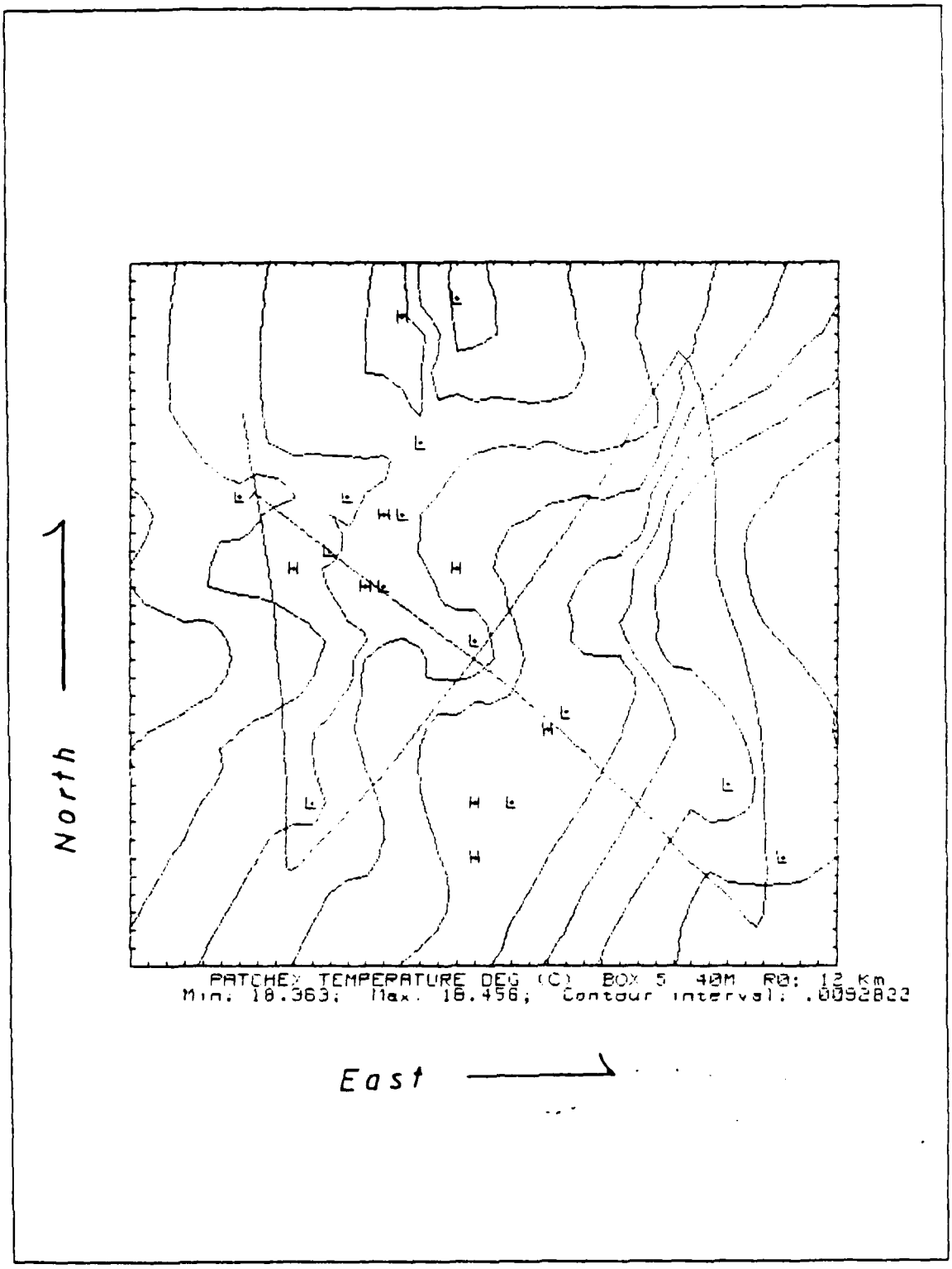

Figure 5.12 40 meter temperature, pattern 5, 14 km N X 14 km E, R_0 = 12 km.

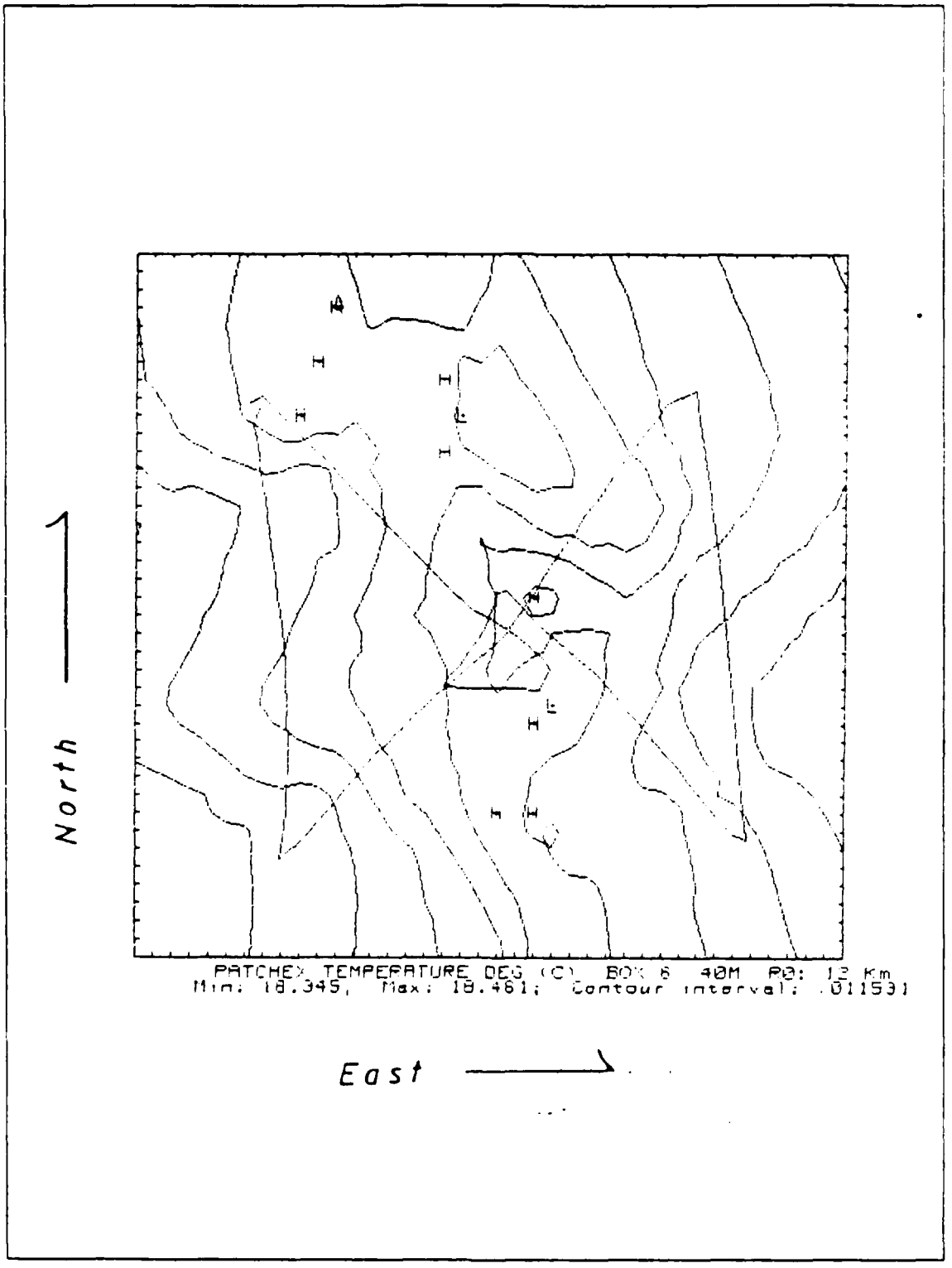

Figure 5.13 40 meter temperature, pattern 6, 14 km N X 14 km E, R_0 = 12 km.

VI. SUMMARY AND RECOMMENDATIONS

The period from 6-12 October 1986, was examined as a subset of the PATCHEX experiment. During this time, there were two distinctly different periods of heat flux and horizontal temperature structure in the mixed layer. To understand the differences between the 6-8 October time-frame and the four days that followed, the surface fluxes, heat content, and horizontally-varying, constant-depth, temperature time series were examined.

The arrival of the R/V POINT SUR was at the end of a period of precipitation. The influence of an intensifying anticyclone sets the stage for the conditions that followed. The wind stress averaged 0.1 N/m^2 until the last day of the study. During the first two days, a -150 to 500 W/m^2 diurnal fluctuation existed in the net surface heat flux. An increasing dewpoint depression over the next 4 days was responsible for periods of over 100 W/m^2 of latent heat loss. The maximum daytime insolation dropped from approximately 600 MJ/m^2 on 6 October abruptly to 150 MJ/m^2 on 9 and 10 October. This kept the surface from regaining the large amount of energy it had lost to latent and sensible heating. Cumulative time series showed a diurnal fluction of ± 5 MJ/m^2 early in the study and a net loss of 35 ± 5 MJ/m^2 by the end of the study.

A detailed vertical and horizontal thermohaline analysis of the mixed layer was undertaken. It suggested that from 06 to 08 October, warmer (0.1°C to).2°C) and less saline (0.04 to 0.16 parts per thousand) water comprised a 10-35 meter surface slab over a fossil mixed layer extending to 42-62 meters depth. During the second part of the study, stirring from a 0.1 N/m^2 mean wind stress, and convective mixing from the large surface heat flux maintained the vertical homogeneity of the mixed layer. The analysis also indicated that the upper thermocline was active. Strong stratification, internal waves, thermohaline intrusions, active mixing, and a 0.3 knot current, several meters below the base of the mixed layer, were noted throughout the study.

One of the most important results of this study was the discovery of horizontal temperature gradients in the time series of temperature at 10 and 40 meters. These gradients at 10 and 40 meters, were overlaid upon a 2-day warming trend followed by 4 days of cooling. These longer term heating and cooling trends, as opposed to the short term trends in the time series, were reflected in the surface fluxes. The horizontal

gradients were strongest from 6-8 October and were different at 10 and 40 meters. At 10 meters they were strongest and increased most rapidly from the northwest to the southeast with decreasing temperature. At 40 meters the gradients were weaker. Also, the increasing of the gradient to the southeast was not observed. After 8 October, convective overturning of the layer reduced the magnitude of the gradients to the order of the temporal noise.

The time series of heat content in the mixed layer showed the same trends as the time series of surface heating and fixed depth temperature over the two periods of the study. During the first period, the heat content increased by approximately 0.5 MJ/m^3, and peaked ober, on 8 October. It then decreased by 0.6-0.8 MJ/m^3 by 12 October. This large heat content loss in the mixed layer balanced well against a 0.7 $\pm$ 0.1 MJ m^3 surface loss, however, the importance of horizontal advection and vertical redistribution from entrainment, were not discounted.

Objective analysis of the 10 meter temperature timeseries on 6 October indicated that a temperature gradient in excess of -0.25 m°C/km existed along the northwest to southeast transect of the area. It persisted, but weakened, in two analyses of later transects. At 40 meters, the gradients were weaker and positive from west to east. After the first two days of the study, the mixed layer was virtually isothermal, and the weak gradients were indiscernable from the high frequency noise in the time series at 10 and 40 meters.

After examining the persistence of temperature gradients in the time series and their further resolution by objective analysis and coupling that information with the vertical thermohaline character of the mixed layer, it appears that from 6-8 October there was a two layer mixed layer. Wind stress and extreme heat loss mixed those layers to a virtually isothermal and isohaline state beyond 8 October. The data suggest a rapidly adjusting density interface originally caused by precipitation and the heating of surface water which is eliminated by wind stress and convective mixing. The study neither confirms the existence of a mesoscale feature nor does it discount their existence. The slope of the maximum temperature gradient (25 m°C km) exceeds that which would be observed in conjunction with a mesoscale feature. It is more likely the result of density compensation at the interface between a pool of fresh surface water and the fossil mixed layer. The existence of that extreme temperature gradient, however, can easily mask the presence of a mesoscale signature. To clarify this matter, it is proposed that the Expendable Current Profiler data, large scale CTD data and

shipboard ADVP be examined to discern the large scale interactions surrounding PATCHEX.

Once the mean velocity field is obtained from FLIP, and when the vertical entrainment velocity can be estimated for the R/V POINT SUR data, a more complete closure of the heat balance in the upper ocean should be attempted. Also, to determine the nature of the internal wave field from the PATCHEX data set (both in space and time) a maximum entropy spectral analysis might be undertaken.

LIST OF REFERENCES

Blanc, T.V., 1987: Accuracy of bulk-method-determined-flux, stability, and sea surface roughness. *J. Geophys. Res.*, **92**, 3867-3876.

Bretherton, F.P., R.E. Davis and C.B. Fandry, 1976: A technique for objective analysis and design of oceanographic experiments applied to MODE-73. *Deep-Sea Res.*, **3**, 559-582.

D'Asaro, E.A., 1985: Upper ocean temperature structure, inertial currents, and Richardson numbers observed during strong meteorological forcing. *J. Phys. Oceanogr.*, **15**, 943-962.

Davis,R.E., R. de Szoeke, D. Halpern and P.P. Niiler, 1981: Variability in the upper ocean during MILE. Part 1: The heat and momentum balances. *Deep Sea Res.*, **28**, 1427-1451.

Gandin, L.S., 1965: Objective Analysis of Meteorological Fields. Israel Program for Scientific Translations, Jerusalem, 242 pp.

Garrett, C.J.R., and W. Munk, 1979: Internal waves in the ocean. *Geophys, Fluid. Dyn.*, **11**, 339-369.

Gill, A.E. 1986: *Atmosphere-Ocean Dynamics.* Academic Press, 662 pp.

Gregg *et al*, 1984: *PATCHEX: An Experiment to Observe Mixing Patches and Internal Waves.* APL, University of Washington, planning guide.

Gregg, M.C., 1984: Persistent turbulent mixing and near-inertial internal waves. *PATCHEX: An Experiment to Observe Mixing Patches and Internal Waves*, November 1984, appendix of pre-prints, 24 pp.

Large, W.G., and S. Pond, 1982: Sensible and latent heat flux measurements over the ocean. *J. Phys. Oceanogr.* **12**, 464-482.

Large, W.G, J.C. McWilliams and P.P. Niiler, 1986: Upper ocean thermal response to strong autumnal forcing of the northeast Pacific. *J. Phys. Oceanogr.*, **16**, 1524-1550.

Panofsky, H.A., and J.A. Dutton, 1987: *Atmospheric Turbulence.* Wiley Interscience, 389 pp.

Paulson, C.A., 1970: Representation of wind speed and temperature profiles in an unstable atmospheric surface layer. *J. Phys. Oceanogr.*, **9**, 857-861.

INITIAL DISTRIBUTION LIST

		No. Copies
1.	Defense Technical Information Center Cameron Station Alexandria, VA 22304-6145	2
2.	Library, Code 0142 Naval Postgraduate School Monterey, CA 93943-5002	2
3.	Chairman (Code 68Co) Department of Oceanography Naval Postgraduate School Monterey, CA 93943	1
4.	Chairman (Code 63Rd) Department of Meteorology Naval Postgraduate School Monterey, CA 93943	1
5.	Dr. E.B. Thornton (Code 68Tm) Department of Oceanography Naval Postgraduate School Monterey, CA 93943	2
6.	Dr. Rowland W. Garwood (Code 68Gd) Department of Oceanography Naval Postgraduate School Monterey, CA 93943	1
7.	LT John J. Murray 240 Second Ave. Frankfort, NY 13340	2
8.	Timothy P. Stanton Department of Oceanography Naval Postgraduate School Monterey, CA 93943	5
9.	Dr. John Trefry Department of Oceanography Florida Institute of Technology Country Club Road Melbourne, FL 32901	1

10.	Mr. Nicholas Shay Department of Meteorology Naval Postgraduate School Monterey, CA 93947	1
11.	Dr. C.N.K. Mooers, Director Institute for Naval Oceanography Room 322, Bldg. 1100 NSTL, MS 39529	1
12.	Director, Naval Oceanography Division Naval Observatory 34th and Massachusetts Avenue NW Washington, DC 20390	1
13.	Commander Naval Oceanography Command NSTL Station Bay St. Louis, MS 39522	1
14.	Commanding Officer Naval Oceanographic Office NSTL Station Bay St. Louis, MS 39522	1
15.	Commanding Officer Fleet Numerical Oceanography Center Monterey, CA 93943	1
16.	Commanding Officer Naval Ocean Research and Development Activity NSTL Station Bay St. Louis, MS 39522	1
17.	Commanding Officer Naval Environmental Prediction Research Facility Monterey, CA 93943	1
18.	Chairman, Oceanography Department U.S. Naval Academy Annapolis, MD 21402	1
19.	Naval Ocean Research and Development Activity 800 N. Quincy Street Arlington, VA 22217	1
20.	Office of Naval Research (Code 420) 800 N. Quincy Street Arlington, VA 22217	1

21. Scientific Liason Office — 1
Office of Naval Research
Scripps Institution of Oceanography
La Jolla, CA 92037

22. Commander — 1
Oceanographic Systems Pacific
Box 1390
Pearl Harbor, HI 96860

23. Commanding Officer — 1
Naval Eastern Oceanography Center
Naval Air Station
Norfolk, VA 23511

24. Commanding Officer — 1
Naval Western Oceanography Center
Box 113
Pearl Harbor, HI 96860

25. Commanding Officer — 1
Naval Oceanography Command Center, Rota
Box 31
FPO San Francisco, CA 09540

26. Commanding Officer — 1
Naval Oceanography Command Center, Guam
Box 12
FPO San Francisco, CA 96630

27. Commanding Officer — 1
Naval Oceanography Command Facility
Cubi Point, RP
FPO San Francisco, CA 96654

28. Officer in Charge — 1
Naval Oceanography Command Detachment
Diego Garcia
Box 10
FPO San Francisco, CA 96685

END

DATE

FILMED

6-1988

DTIC